NASA/TM–20220016410

Structural Model Tuning Tool: User's Reference Manual

Chan-gi Pak
Armstrong Flight Research Center, Edwards, California

December 2022

NASA STI Program Report Series

The NASA STI Program collects, organizes, provides for archiving, and disseminates NASA's STI. The NASA STI program provides access to the NTRS Registered and its public interface, the NASA Technical Reports Server, thus providing one of the largest collections of aeronautical and space science STI in the world. Results are published in both non-NASA channels and by NASA in the NASA STI Report Series, which includes the following report types:

- TECHNICAL PUBLICATION. Reports of completed research or a major significant phase of research that present the results of NASA Programs and include extensive data or theoretical analysis. Includes compilations of significant scientific and technical data and information deemed to be of continuing reference value. NASA counterpart of peer-reviewed formal professional papers but has less stringent limitations on manuscript length and extent of graphic presentations.

- TECHNICAL MEMORANDUM. Scientific and technical findings that are preliminary or of specialized interest, e.g., quick release reports, working papers, and bibliographies that contain minimal annotation. Does not contain extensive analysis.

- CONTRACTOR REPORT. Scientific and technical findings by NASA-sponsored contractors and grantees.

- CONFERENCE PUBLICATION. Collected papers from scientific and technical conferences, symposia, seminars, or other meetings sponsored or co-sponsored by NASA.

- SPECIAL PUBLICATION. Scientific, technical, or historical information from NASA programs, projects, and missions, often concerned with subjects having substantial public interest.

- TECHNICAL TRANSLATION. English-language translations of foreign scientific and technical material pertinent to NASA's mission.

Specialized services also include organizing and publishing research results, distributing specialized research announcements and feeds, providing information desk and personal search support, and enabling data exchange services.

For more information about the NASA STI program, see the following:

- Access the NASA STI program home page at http://www.sti.nasa.gov

- Help desk contact information:

https://www.sti.nasa.gov/sti-contact-form/
and select the "General" help request type.

NASA/ TM–20220016410

Structural Model Tuning Tool: User's Reference Manual

Chan-gi Pak
Armstrong Flight Research Center, Edwards, California

National Aeronautics and
Space Administration

Armstrong Flight Research Center
Edwards, California, 93534-0273

December 2022

Acknowledgments

The work presented in this report was funded by the Low-Boom Flight Demonstration Project under the National Aeronautics and Space Administration Aeronautics Research Mission Directorate. The author thanks peer review committee members Samson Truong, Benjamin Park, and Scott L. Stebbins of the National Aeronautics and Space Administration Armstrong Flight Research Center.

This report is available in electronic form at

https://ntrs.nasa.gov

Abstract

This report presents an efficient approach for tuning finite element models to match the measured ground vibration test and static test data. Frequencies, mode shapes, total weight, location of the center of gravity, and static deformation computed from the finite element model are matched to the measured data. The model tuning procedure used in this work is based on solving an optimization problem in which the errors for the considered metrics, between the finite element prediction and the measured data, are minimized. Analytical sensitivity values of performance indices are computed using the NASTRAN-generated sensitivity values together with the in-house computer codes, which allow for faster computational time and the use of gradient-based optimizers. The method is applied to the Aerostructures Test Wing IV model. The study shows that the military standard and the National Aeronautics and Space Administration standard for comparing analytical and experimental modal data are all satisfied. The final finite element model correlates well with the test data. The flutter speed decreases by 8.91 percent after model tuning compared with the original Aerostructures Test Wing IV design.

Nomenclature

Acronyms

AFRC	Armstrong Flight Research Center
AOM	auto-orthogonality matrix (or orthonormalized mass matrix)
ATW	Aerostructures Test Wing
CG	center of gravity
COM	cross-orthogonality matrix (or mode shape matrix)
DOF	degrees of freedom
FE	finite element
FOM	full-order model
GVT	ground vibration test
KEAS	knots equivalent air speed
MAC	modal assurance criteria
NASA	National Aeronautics and Space Administration
ROM	reduced order model
SEREP	System Equivalent Reduction Expansion Process
STTR	Small Business Technology Transfer
V-f	velocity vs. frequency
V-g	velocity vs. structural damping

Symbols

F_{ir}	i-th reference response function value for computation of i-th performance index
$F_i(x_k)$	i-th response function computed from NASTRAN solution 200
f_j	j-th analytical frequency, Hz
f_{jG}	j-th measured frequency, Hz
$\boldsymbol{I}$	identity matrix
I_{xxG}	moment of inertia I_{xx} with respect to CG
I_{xxo}	moment of inertia I_{xx} with respect to origin
I_{yxG}	moment of inertia I_{yx} with respect to CG
I_{yxo}	moment of inertia I_{yx} with respect to origin
I_{yyG}	moment of inertia I_{yy} with respect to CG
I_{yyo}	moment of inertia I_{yy} with respect to origin

I_{zxG}	moment of inertia I_{zx} with respect to CG
I_{zxo}	moment of inertia I_{zx} with respect to origin
I_{zyG}	moment of inertia I_{zy} with respect to CG
I_{zyo}	moment of inertia I_{zy} with respect to origin
I_{zzG}	moment of inertia I_{zz} with respect to CG
I_{zzo}	moment of inertia I_{zz} with respect to origin
J	objective function
J_i	i-th performance indices
m	number of modes to be matched
n_{FDOF}	number of full-order DOF
n_{MDOF}	number of measured DOF
n_{RDOF}	number of reduced DOF
W	total weight
W_G	measured total weight
x_{CG}	X-CG location
x_k	k-th design variable
x_{MCG}	measured X-CG location
y_{CG}	Y-CG location
y_{MCG}	measured Y-CG location
z_{CG}	Z-CG location
z_{MCG}	measured Z-CG location
$\boldsymbol{M_{AOM}}$	auto-orthogonality matrix
$\boldsymbol{M_{COM}}$	cross-orthogonality matrix
$\mathbf{M}_R$	reduced order mass matrix
$\mathbf{T}$	transformation matrix, full-order DOF to reduced order DOF
$\boldsymbol{\omega}_n$	natural frequency
$\boldsymbol{\Psi}_R$	intermediate matrix to compute $\boldsymbol{M}_R$
$\boldsymbol{\Psi}_M$	intermediate matrix to compute $\boldsymbol{\Phi}_{GR}$
$\boldsymbol{\Phi}_M$	eigenmatrix, corresponds to master (or measured) DOF
$\widetilde{\boldsymbol{\Phi}}_{GM}$	measured eigenmatrix
$\boldsymbol{\Phi}_{GR}$	expanded eigenmatrix
$\boldsymbol{\Phi}_R$	eigenmatrix, corresponds to reduced DOF
$\boldsymbol{\Phi}_S$	eigenmatrix, corresponds to slave DOF
$(*)^T$	transpose of a matrix
$(*)^{-1}$	inverse of a matrix
$\frac{\partial(*)}{\partial x_k}$	sensitivity value with respect to the k-th design variable x_k

Introduction

Generally, structural dynamic finite element (FE) models for production aircraft need to be correlated to the measured data to ensure the accuracy of the numerical models. A trial-and-error approach for structural model tuning remains the most popular methodology in industry and government to save aircraft development schedule time between the ground vibration test and the first flight test. The quality of the tuned FE model is, therefore, questionable for its use in predicting aeroelastic and aeroservoelastic behavior during flight. Tuning the FE model using measured data has been a challenging problem in structural dynamics for more than five decades. There has been great effort in the past couple of decades in developing methods to update these FE models to match computed frequencies and mode shapes to the measured ground vibration test (GVT) data (refs. 1-5). An FE model tuning tool using GVT data has also been developed at the National Aeronautics and Space Administration

(NASA) Armstrong Flight Research Center (AFRC) (refs. 6–8) to minimize uncertainties in an analytical FE model. Most recent efforts to address this problem have focused on applying similar techniques to the health monitoring of structures (refs. 9–12). Literature surveys on the FE model tuning are summarized in refs. 13-15.

An FE model tuning of an aircraft is critical to having accurate aeroelastic and aeroservoelastic behavior during flight. When computed modes are not accurately correlated with measured GVT data, there can be significant and unknown inaccuracies in the results from dynamic load, flutter (ref. 7), or aeroservoelastic stability analyses. These errors can be caused by differences in mode shapes or modal frequencies; thus, the correlation procedures used to match the GVT data and computed modes should include both natural frequencies and mode shapes. The general perception is that any discrepancies between tests and analysis are due solely to modeling uncertainties. Errors in measured modal data are also associated with sensor reliability; sensor/actuator installation; supporting structures; measurement noise; curve fitting; or the experimentalist performing modal tests (ref. 15).

The primary objective of this study is to develop and validate a straight-forward and efficient technique for inclusion of the measured test data into the FE model. Calculations of the objective function and constraints require a full FE analysis; this calculation process is time-consuming and expensive, especially when many iterations are required for optimization of a complex FE model. When using gradient-based optimization algorithms, using finite differences to calculate derivatives (refs. 6-8) makes the required computational time even longer. Presented in this report is a computational approach to model tuning that employs analytical sensitivities for error indices based on the MSC NASTRAN code (Hexagon, Stockholm, Sweden) (ref. 16) and in-house pre- and post-processor codes. During each design cycle, the set of design variables and constraints is redefined to improve the efficiency of the proposed approach. Accordingly, the efficiency of the method is increased, which also provides an incremental framework that allows for a faster, less-computationally-expensive model tuning procedure.

Mathematical Backgrounds

The mathematical equations for performance indices and their corresponding analytical sensitivity values will be derived in this section. These performance indices and sensitivity values are computed using the MSC NASTRAN code (ref. 16) with in-house computer codes. The following performance indices will be used for the structural model tuning procedure:

1) Total weight.
2) Center of gravity (CG) location.
3) Mass moment of inertias (if test data are available).
4) Static deformation under multiple load cases.
5) Frequencies.
6) Orthonormalized mass matrix or auto-orthogonality matrix (AOM).
7) Mode shape matrix or cross-orthogonality matrix (COM).

Figure 1 shows the pre-processor, the analyzer, and the post-processor modules. The “update NASTRAN input” belongs to a pre-procedure module. This study uses the MSC NASTRAN analysis with a single iteration of solution 200 (optimization), selected analyzer module, as shown in fig. 1. The MSC NASTRAN calculates response function values and sensitivity values of response functions. The post-processor modules compute performance indices and their sensitivity values.

Weight Module

Total weight W and weight sensitivity values with respect to a design variable x_k, $\frac{\partial W}{\partial x_k}$, are obtained using the NASTRAN code. The performance index for the total weight, J_1 (ref. 8), and corresponding sensitivity value $\frac{\partial J_1}{\partial x_k}$ are obtained using eqs. (1) and (2):

i-th performance index
$$J_i = \left(\frac{F_i(x_k) - F_{ir}}{F_{ir}}\right)^2 \tag{1}$$

Sensitivity value of J_i
$$\frac{\partial J_i}{\partial x_k} = 2\left(\frac{F_i(x_k) - F_{ir}}{F_{ir}}\right)\left(\frac{1}{F_{ir}}\right)\frac{\partial F_i(x_k)}{\partial x_k} \tag{2}$$

where, F_{1r} is the measured weight W_G and $F_1(x_k)$ and $\frac{\partial F_1(x_k)}{\partial x_k}$ are W and $\frac{\partial W}{\partial x_k}$, respectively.

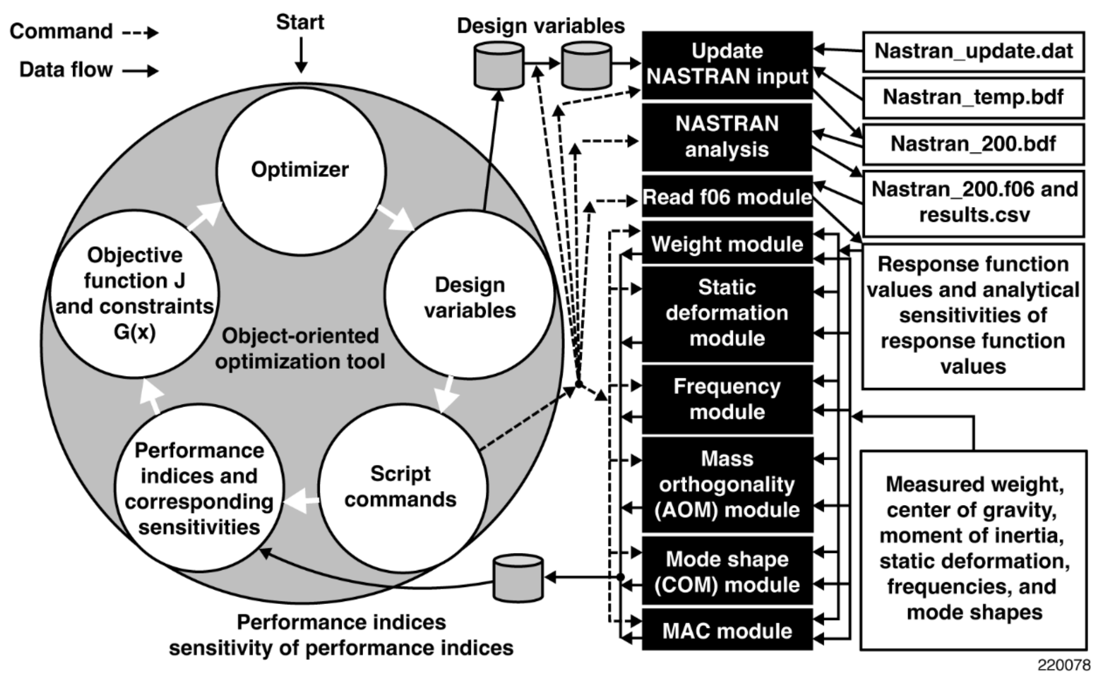

Figure 1. Block diagram of analytical sensitivity-based structural model tuning tool.

The six-by-six weight information with respect to the reference point "o" from the NASTRAN output is given in eq. (3):

$$[W] = \begin{bmatrix} W_{11} & W_{12} & W_{13} & W_{14} & W_{15} & W_{16} \\ W_{21} & W_{22} & W_{23} & W_{24} & W_{25} & W_{26} \\ W_{31} & W_{32} & W_{33} & W_{34} & W_{35} & W_{36} \\ W_{41} & W_{42} & W_{43} & W_{44} & W_{45} & W_{46} \\ W_{51} & W_{52} & W_{53} & W_{54} & W_{55} & W_{56} \\ W_{61} & W_{62} & W_{63} & W_{64} & W_{65} & W_{66} \end{bmatrix}$$
$$= \begin{bmatrix} W & 0 & 0 & 0 & Wz_{CG} & -Wy_{CG} \\ 0 & W & 0 & -Wz_{CG} & 0 & Wx_{CG} \\ 0 & 0 & W & Wy_{CG} & -Wx_{CG} & 0 \\ 0 & -Wz_{CG} & Wy_{CG} & I_{xxo} & I_{xyo} & I_{xzo} \\ Wz_{CG} & 0 & -Wx_{CG} & I_{yxo} & I_{yyo} & I_{yzo} \\ -Wy_{CG} & Wx_{CG} & 0 & I_{zxo} & I_{zyo} & I_{zzo} \end{bmatrix} \tag{3}$$

The CG location, therefore, can be obtained using eq. (4):

$$\begin{aligned} x_{CG} &= \frac{W_{26}}{W} \\ y_{CG} &= \frac{W_{34}}{W} \\ z_{CG} &= \frac{W_{15}}{W} \end{aligned} \tag{4}$$

The response function values x_{CG}, y_{CG}, and z_{CG}, and corresponding sensitivity values $\frac{\partial x_{CG}}{\partial x_k}$, $\frac{\partial y_{CG}}{\partial x_k}$, and $\frac{\partial z_{CG}}{\partial x_k}$ are defined and computed using the NASTRAN solution 200 with bulk data entries DRESP1, DRESP2, and DEQATN (ref. 16); therefore, performance indices J_i $i = 2, 3,$ and 4, and corresponding sensitivity values $\frac{\partial J_i}{\partial x_k}$ are also computed using eqs. (1) and (2) as well as x_{CG}, y_{CG}, z_{CG}, $\frac{\partial x_{CG}}{\partial x_k}$, $\frac{\partial y_{CG}}{\partial x_k}$, and $\frac{\partial z_{CG}}{\partial x_k}$.
The measured CG locations x_{MCG}, y_{MCG}, and z_{MCG} are the reference values F_{2r}, F_{3r}, and F_{4r} in this computation.

The diagonal terms of the mass moment of inertia matrix with respect to the CG location are computed using eqs. (5)-(7):

$$I_{xxG} = I_{xxo} - W({y_{CG}}^2 + {z_{CG}}^2) = W_{44} - W({y_{CG}}^2 + {z_{CG}}^2) \tag{5}$$

$$I_{yyG} = I_{yyo} - W({z_{CG}}^2 + {x_{CG}}^2) = W_{55} - W({z_{CG}}^2 + {x_{CG}}^2) \tag{6}$$

$$I_{zzG} = I_{zzo} - W({x_{CG}}^2 + {y_{CG}}^2) = W_{66} - W({x_{CG}}^2 + {y_{CG}}^2) \tag{7}$$

Based on the NASTRAN compatible sign convention, the off-diagonal terms of the mass moment of inertia matrix are expressed in eqs. (8)-(10):

$$I_{xyG} = I_{xyo} - W \times x_{CG} \times y_{CG} = -W_{45} - W \times x_{CG} \times y_{CG} \tag{8}$$

$$I_{yzG} = I_{yzo} - W \times y_{CG} \times \mathrm{z}_{CG} = -W_{56} - W \times y_{CG} \times \mathrm{z}_{CG} \tag{9}$$

$$I_{zxG} = I_{zxo} - W \times z_{CG} \times x_{CG} = -W_{64} - W \times z_{CG} \times x_{CG} \tag{10}$$

Performance indices J_i $i = 5, \ldots,$ and 10, and corresponding sensitivity values, $\frac{\partial J_i}{\partial x_k}$, for mass moment of inertias can also be obtained using eqs. (1) and (2) together with the NASTRAN computed response function values I_{xxG}, I_{yyG}, I_{zzG}, I_{xyG}, I_{yzG}, and I_{zxG}; corresponding sensitivity values $\frac{\partial I_{xxG}}{\partial \mathrm{x}_k}$, $\frac{\partial I_{yyG}}{\partial \mathrm{x}_k}$, $\frac{\partial I_{zzG}}{\partial \mathrm{x}_k}$, $\frac{\partial I_{xyG}}{\partial \mathrm{x}_k}$, $\frac{\partial I_{yzG}}{\partial \mathrm{x}_k}$, and $\frac{\partial I_{zxG}}{\partial \mathrm{x}_k}$; and the measured reference values I_{xxMG}, I_{yyMG}, I_{zzMG}, I_{xyMG}, I_{yzMG}, and I_{zxMG}.

Frequency Module

In this study, it is assumed that the m number of analytical frequencies f_j $j = 1, 2, \ldots, m$ will be matched to the m-measured GVT frequencies f_{jG} $j = 1, 2, \ldots, m$. Initially, these frequencies (response function values) f_j $j = 1, 2, \ldots, m$, and corresponding sensitivity values $\frac{\partial f_j}{\partial \mathrm{x}_k}$ are computed using the NASTRAN solution 200. Next, performance indices J_i $i = 11, 12$, and $10 + m$, and corresponding sensitivity values, $\frac{\partial J_i}{\partial x_k}$, are computed using eqs. (1) and (2). In this case, the reference values, F_{ir}, are the m measured GVT frequencies, f_{jG} $j = 1, 2, \ldots, m$.

Orthogonality Module

The AOM and COM are computed using eqs. (11) and (12), respectively (ref. 8):

$$\boldsymbol{M_{AOM}} = \mathbf{\Phi}_{GR}^{\mathrm{T}} \mathbf{M}_R \mathbf{\Phi}_{GR} \qquad \text{(order = } m \times m\text{)} \tag{11}$$

$$\boldsymbol{M_{COM}} = \mathbf{\Phi}_{GR}^{\mathrm{T}} \mathbf{M}_R \mathbf{\Phi}_{R} \qquad \text{(order = } m \times m\text{)} \tag{12}$$

The detailed derivation of the System Equivalent Reduction Expansion Process (SEREP) (ref. 17) is given in Appendix A where the order of a reduced order mass matrix $\mathbf{M}_R$ in eq. (13) is based on reduced degrees of freedom (DOF).

$$\mathbf{M}_R = \mathbf{\Psi}_R^T \mathbf{\Psi}_R \qquad \text{(order = } n_{RDOF} \times n_{RDOF}\text{)} \tag{13}$$

The matrix $\mathbf{\Psi}_R$ in eq. (14) is used for the transformation matrix $\mathbf{T}$ of the SEREP, as shown in eq. (15):

$$\mathbf{\Psi}_R = \left(\mathbf{\Phi}_R^{\mathrm{T}} \mathbf{\Phi}_R\right)^{-1} \mathbf{\Phi}_R^{\mathrm{T}} \qquad \text{(order = } m \times n_{RDOF}\text{)} \tag{14}$$

$$\mathbf{T} = \mathbf{\Phi} \mathbf{\Psi}_R \qquad \text{(order = } n_{FDOF} \times n_{RDOF}\text{)} \tag{15}$$

In eq. (16), matrices $\mathbf{\Phi}_M$ (order = $n_{MDOF} \times m$) and $\mathbf{\Phi}_S$ (order = $(n_{RDOF} - n_{MDOF}) \times m$) are the master and slave eigen matrices. From eqs. (13) and (14), reduced order mass matrix $\mathbf{M}_R$ and $\mathbf{\Phi}_R$ satisfy eq. (17):

$$\mathbf{\Phi}_R \equiv \begin{bmatrix} \mathbf{\Phi}_M \\ \mathbf{\Phi}_S \end{bmatrix} \qquad \text{(order = } n_{RDOF} \times m\text{)} \tag{16}$$

$$\mathbf{\Phi}_R^{\mathrm{T}} \mathbf{M}_R \mathbf{\Phi}_R = \boldsymbol{I} \qquad \text{(order = } m \times m\text{)} \tag{17}$$

The matrix $\widetilde{\Phi}_{GM}$ (order = $n_{MDOF} \times m$) in eq. (18) is the measured eigenmatrix obtained from the GVT. The row DOF n_{MDOF} should be expanded to the reduced DOF n_{RDOF} to perform the matrix triple-multiplications in eqs. (11) and (12). An expanded eigenmatrix Φ_{GR} is also computed using SEREP, as shown in eq. (18). The matrix $\mathbf{\Psi}_M$ in eq. (18) is given in eq. (19):

$$\mathbf{\Phi}_{GR} = \begin{bmatrix} \mathbf{\Phi}_M \mathbf{\Psi}_M \\ \mathbf{\Phi}_S \mathbf{\Psi}_M \end{bmatrix} \widetilde{\mathbf{\Phi}}_{GM} \qquad \text{(order = } n_{RDOF} \times m\text{)} \tag{18}$$

$$\mathbf{\Psi}_M = \left(\mathbf{\Phi}_M^{\mathrm{T}} \mathbf{\Phi}_M\right)^{-1} \mathbf{\Phi}_M^{\mathrm{T}} \qquad \text{(order = } m \times n_{MDOF}\text{)} \tag{19}$$

In this study, this expanded eigenmatrix $\mathbf{\Phi}_{GR}$ is normalized with respect to the reduced order mass matrix $\mathbf{M}_R$ in eq. (11) once at the start of the design configuration, then it will be assumed that $\mathbf{\Phi}_{GR}$ is constant during the optimization cycle. The numbers n_{RDOF} and n_{MDOF} are the number of the reduced DOF, and the number of the master (or measured) DOF, respectively.

Diagonal and off-diagonal terms of matrices $\boldsymbol{M_{AOM}}$ and $\boldsymbol{M_{COM}}$ are selected as performance indices. First, a response function value Φ_R (reduced order eigenmatrix) and corresponding sensitivity matrix $\frac{\partial \Phi_R}{\partial x_k}$ are obtained from the NASTRAN code.

The sensitivity matrices $\frac{\partial \boldsymbol{M_{AOM}}}{\partial x_k}$ and $\frac{\partial \boldsymbol{M_{COM}}}{\partial x_k}$ from eqs. (11) and (12) become eqs. (20) and (21), respectively:

$$\frac{\partial \boldsymbol{M_{AOM}}}{\partial x_k} = \frac{\partial \mathbf{\Phi}_{GR}^{\mathrm{T}} \mathbf{M}_R \mathbf{\Phi}_{GR}}{\partial x_k} = \mathbf{\Phi}_{GR}^{\mathrm{T}} \frac{\partial \mathbf{M}_R}{\partial x_k} \mathbf{\Phi}_{GR} \tag{20}$$

$$\frac{\partial \boldsymbol{M_{COM}}}{\partial x_k} = \frac{\partial \mathbf{\Phi}_{GR}^{\mathrm{T}} \mathbf{M}_R \mathbf{\Phi}_R}{\partial x_k} = \mathbf{\Phi}_{GR}^{\mathrm{T}} \frac{\partial \mathbf{M}_R}{\partial x_k} \mathbf{\Phi}_R + \mathbf{\Phi}_{GR}^{\mathrm{T}} \mathbf{M}_R \frac{\partial \mathbf{\Phi}_R}{\partial x_k} \tag{21}$$

The sensitivity matrix $\frac{\partial \Phi_R}{\partial x_k}$ in eq. (21) is directly obtained from the NASTRAN computation as mentioned before; therefore, $\frac{\partial \mathbf{M}_R}{\partial x_k}$ should be computed to have $\frac{\partial \boldsymbol{M_{AOM}}}{\partial x_k}$ and $\frac{\partial \boldsymbol{M_{COM}}}{\partial x_k}$ values. First, $\frac{\partial \mathbf{M}_R}{\partial x_k}$ in eqs. (20) and (21) is derived as in eq. (22) using eq. (13):

$$\frac{\partial \mathbf{M}_R}{\partial x_k} = \frac{\partial \mathbf{\Psi}_R^T}{\partial x_k} \left(\mathbf{\Phi}_R^{\mathrm{T}} \mathbf{\Phi}_R\right)^{-1} \mathbf{\Phi}_R^{\mathrm{T}} + \mathbf{\Phi}_R \left(\mathbf{\Phi}_R^{\mathrm{T}} \mathbf{\Phi}_R\right)^{-\mathrm{T}} \frac{\partial \mathbf{\Psi}_R}{\partial x_k} \tag{22}$$

The sensitivity of $\mathbf{\Psi}_R$ in eq. (14) is derived as in eq. (23). The details are given in Appendix B:

$$\frac{\partial \mathbf{\Psi}_R}{\partial x_k} = \left(\mathbf{\Phi}_R^{\mathrm{T}} \mathbf{\Phi}_R\right)^{-1} \frac{\partial \mathbf{\Phi}_R^{\mathrm{T}}}{\partial x_k} - \left(\mathbf{\Phi}_R^{\mathrm{T}} \mathbf{\Phi}_R\right)^{-1} \left(\frac{\partial \mathbf{\Phi}_R^{\mathrm{T}}}{\partial x_k} \mathbf{\Phi}_R + \mathbf{\Phi}_R^{\mathrm{T}} \frac{\partial \mathbf{\Phi}_R}{\partial x_k}\right) \left(\mathbf{\Phi}_R^{\mathrm{T}} \mathbf{\Phi}_R\right)^{-1} \mathbf{\Phi}_R^{\mathrm{T}} \tag{23}$$

therefore, the matrix $\frac{\partial \mathbf{M}_R}{\partial x_k}$ in eqs. (20) and (21) becomes eq. (24):

$$\frac{\partial \mathbf{M}_R}{\partial x_k} = \left[\left(\mathbf{\Phi}_R^{\mathrm{T}}\mathbf{\Phi}_R\right)^{-1}\frac{\partial \mathbf{\Phi}_R^{\mathrm{T}}}{\partial x_k} - \left(\mathbf{\Phi}_R^{\mathrm{T}}\mathbf{\Phi}_R\right)^{-1}\left(\frac{\partial \mathbf{\Phi}_R^{\mathrm{T}}}{\partial x_k}\mathbf{\Phi}_R + \mathbf{\Phi}_R^{\mathrm{T}}\frac{\partial \mathbf{\Phi}_R}{\partial x_k}\right)\left(\mathbf{\Phi}_R^{\mathrm{T}}\mathbf{\Phi}_R\right)^{-1}\mathbf{\Phi}_R^{\mathrm{T}}\right]^{\mathrm{T}}\left(\mathbf{\Phi}_R^{\mathrm{T}}\mathbf{\Phi}_R\right)^{-1}\mathbf{\Phi}_R^{\mathrm{T}}$$
$$+\mathbf{\Phi}_R\left(\mathbf{\Phi}_R^{\mathrm{T}}\mathbf{\Phi}_R\right)^{-\mathrm{T}}\left[\left(\mathbf{\Phi}_R^{\mathrm{T}}\mathbf{\Phi}_R\right)^{-1}\frac{\partial \mathbf{\Phi}_R^{\mathrm{T}}}{\partial x_k} - \left(\mathbf{\Phi}_R^{\mathrm{T}}\mathbf{\Phi}_R\right)^{-1}\left(\frac{\partial \mathbf{\Phi}_R^{\mathrm{T}}}{\partial x_k}\mathbf{\Phi}_R + \mathbf{\Phi}_R^{\mathrm{T}}\frac{\partial \mathbf{\Phi}_R}{\partial x_k}\right)\left(\mathbf{\Phi}_R^{\mathrm{T}}\mathbf{\Phi}_R\right)^{-1}\mathbf{\Phi}_R^{\mathrm{T}}\right] \tag{24}$$

The performance indices J_{ij}, for each off-diagonal element of the AOM and COM in eqs. (11) and (12), respectively and corresponding sensitivity value $\frac{\partial J_{ij}}{\partial x_k}$ are obtained using eqs. (25) and (26):

$$J_{ij} \equiv {m_{ij}}^2 \tag{25}$$

$$\frac{\partial J_{ij}}{\partial x_k} = 2m_{ij}\frac{\partial m_{ij}}{\partial x_k} \tag{26}$$

where, an off-diagonal term m_{ij} is the i-th row and j-th column element of the AOM ($\boldsymbol{M_{AOM}}$), or COM ($\boldsymbol{M_{COM}}$). Similarly, $\frac{\partial m_{ij}}{\partial x_k}$ is the i-th row and j-th column element of $\frac{\partial \boldsymbol{M_{AOM}}}{\partial x_k}$ or $\frac{\partial \boldsymbol{M_{COM}}}{\partial x_k}$.

The performance indices J_{ii}, for each diagonal element of the COM in eq. (12) and corresponding sensitivity value $\frac{\partial J_{ii}}{\partial x_k}$ are obtained using eqs. (27) and (28):

$$J_{ii} \equiv 1 - {m_{ii}}^2 \tag{27}$$

$$\frac{\partial J_{ii}}{\partial x_k} = -2m_{ii}\frac{\partial m_{ii}}{\partial x_k} \tag{28}$$

Static Deformation Module

A static deformation and corresponding sensitivity values are also computed using the NASTRAN code. The performance index J_{Li} for the i-th load case and corresponding sensitivity value with respect to a design variable x_k, $\frac{\partial J_{Li}}{\partial x_k}$, are obtained using eqs. (29) and (30):

Performance index for the i-th load case
$$J_{Li} = \frac{1}{m_p}\sum_{j=1}^{m_p}\left(\Delta_{ij} - \Delta_{ijT}\right)^2 \tag{29}$$

Sensitivity value of J_{Li}
$$\frac{\partial J_{Li}}{\partial x_k} = \frac{1}{m_p}\sum_{j=1}^{m_p} 2\left(\Delta_{ij} - \Delta_{ijT}\right)\frac{\partial \Delta_{ij}}{\partial x_k} \tag{30}$$

where, Δ_{ijT} and Δ_{ij} are the measured and corresponding analytical deformations at the j-th deformation sensor under the i-th load condition, respectively; and m_p is the total number of deformation sensors during static tests such as proof and calibration tests. The deformation values Δ_{ij} and corresponding sensitivity values $\frac{\partial \Delta_{ij}}{\partial x_k}$ are obtained using the NASTRAN solution 200.

Numerical Validation of New Structural Model Tuning Tool

The MSC NASTRAN commands for the computation of response functions and corresponding sensitivity values are summarized in Appendix C. A sample input deck for MSC NASTRAN solution 200 is also prepared in Appendix D.

This section validates the structural model tuning tool with analytical sensitivity values. The example problem is based on a cantilevered Aerostructures Test Wing (ATW) IV model.

Structural Dynamic Model Tuning of the Cantilevered Aerostructures Test Wing IV Model

The two variants of the ATW IV, baseline and curvilinear spars and ribs (SpaRibs) (ref. 18), have been manufactured under two NASA Small Business Technology Transfer (STTR contract numbers: NNX14CD16P and NNX15CD08C). In this study, the baseline ATW IV is chosen as an example.

Correlation of the Baseline Aerostructures Test Wing IV Model with Respect to Ground Vibration Test Data

The GVT has been performed to validate the FE model of the baseline ATW IV. The grid numbers with accelerometer direction and geometric locations are given in table 1 and fig. 2(a). The PCB® (PCB Piezotronics, Inc.) (Depew, New York) tri-axial and miniature teardrop accelerometers are used on the mounting table and test article, respectively, as shown in figs. 2(b) and 2(c). Figure 2(b) shows two tri-axial accelerometers are used to monitor the movement of the mounting table. Impulse testing with the PCB® 086C02 impulse hammer (figs. 2(c) and 2(d)) has been performed. The out-of-plane (Z direction) excitation is hit right next to the accelerometer position 3, as shown in figs. 2(a) and 2(c). On the other hand, position 11 in figs. 2(a) and 2(d) is hit for the in-plane (X direction) excitation.

Table 1. Geometric locations of accelerometers.

Accelerometer number	Grid number with (DOF)	X coordinate (in)	Y coordinate (in)	Z coordinate (in)
1	1847 (Z)	9.93	7.20	.19
2	2315 (Z)	13.58	10.8	.17
3	1484 (Z)	17.22	14.4	.16
4	1370 (Z)	15.14	3.60	.03
5	2232 (Z)	18.06	7.20	.03
6	2606 (Z)	20.99	10.8	.03
7	1754 (Z)	23.92	14.4	.03
8	2 (Z)	12.75	18.5	0
9	31 (Z)	32.83	18.5	0
10	2 (X)	12.75	18.5	0
11	31 (X)	32.83	18.5	0

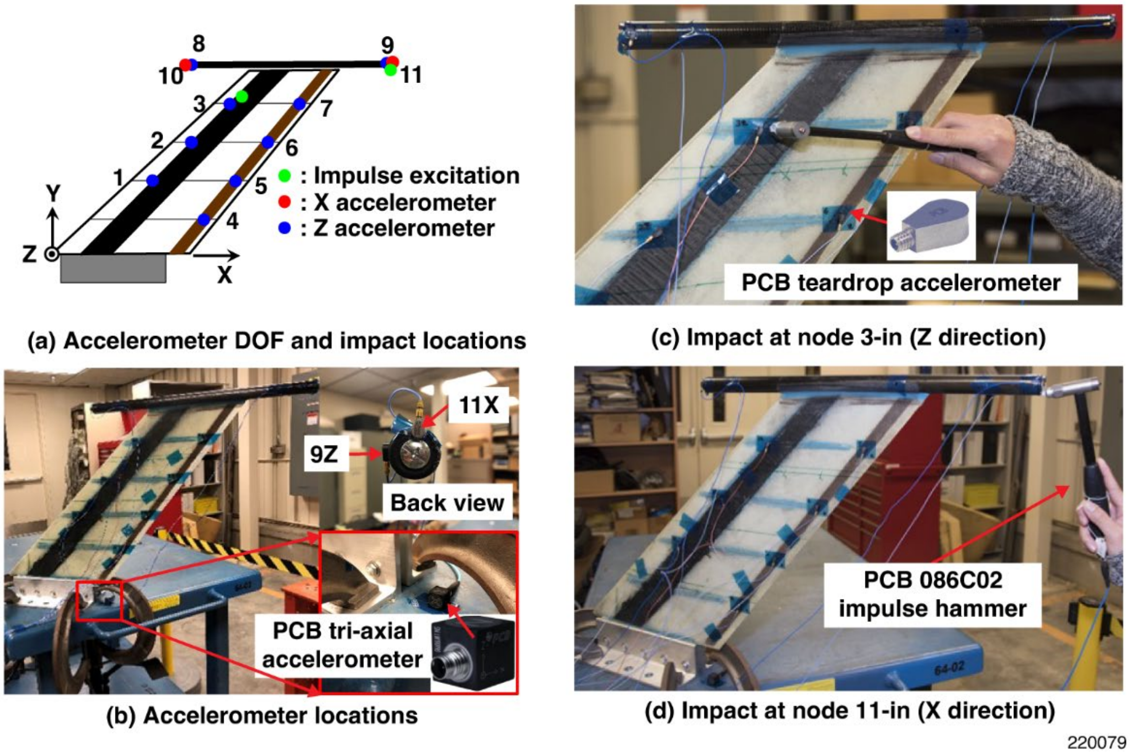

Figure 2. Ground vibration test of the baseline Aerostructures Test Wing IV.

The first five measured frequencies, except Mode 4, are given in the top half section of table 2, third column. Measured weight and X- and Y-CG positions, without the aluminum L-bracket in fig. 3(a) are also provided in table 2. Natural frequencies of the baseline ATW IV model in fig. 3(a) are given in the top half section of table 2, fourth and fifth columns. Corresponding AOM and COM that were obtained from the GVT correlation study are provided in table 3. An unsteady aerodynamic model with spline points for the flutter analysis using the ZAERO (ZONA Technology, Inc.) (Scottsdale, Arizona) code (ref. 19) is also given in fig. 3(b). The flutter speed and frequency of the baseline ATW IV at Mach 0.75 are shown in table 4, second column. Modal participation factors for the primary flutter mode at Mach 0.75 are shown in table 2, second column. The most important modes for the primary flutter mode are the Modes (1, 2, 3, and 5), as shown in table 2. These four modes cover 100 percent of the primary flutter mode; therefore, these four modes are selected as the primary modes for model tuning. Figures 4(a) and 4(b) show the V-g and V-f curves obtained from the flutter analysis prior to model tuning. Huge frequency errors (noted in table 2) for the primary modes 17.8, 13.5, and 7.38 percent are observed with the baseline ATW IV configuration; all of the off-diagonal terms of the AOM (except the third row and first column element in table 3), and half of the off-diagonal terms of the COM, violate 10-percent military and NASA requirements. Because all of the diagonal terms of the COM violate the 90-percent requirement, structural dynamic model tuning is required to have a reliable flutter boundary.

Table 2. Weight; center of gravity; and natural frequencies of example problem.

	MPF[a]	GVT	Baseline model		Delivered model		Fixed model	
			FEM	% Error	FEM	% Error	FEM	% Error
Weight (lb)	N/A	1.686	1.742	3.33	1.742	3.33	1.744	3.43
X-CG (in)		13.37	13.67	2.24	13.67	2.24	13.64	2.01
Y-CG (in)		7.763	7.944	2.33	7.944	2.33	7.934	2.20
Mode 1 (Hz)	5.37%	14.65	17.26	17.8	14.62	-0.17	15.17	3.55
Mode 2 (Hz)	93.5%	29.55	33.54	13.5	29.15	-1.36	30.08	1.79
Mode 3 (Hz)	0.87%	84.92	91.18	7.38	77.37	-8.89	81.01	-4.60
Mode 5 (Hz)	0.27%	181.8	184.5	1.47	158.9	-12.6	175.3	-3.58
Mode 6 (Hz)	0.00%	210.7	228.0	8.21	194.0	-7.92	198.8	-5.65
	After iteration 1		**After iteration 2**		**After iteration 3**		**After iteration 4**	
	FEM	**% Error**	**FEM**	**% Error**	**FEM**	**% Error**	**FEM**	**% Error**
Weight (lb)	1.686	0.00	1.721	2.05	1.726	2.39	1.706	1.17
X-CG (in)	13.55	1.32	13.71	2.51	13.79	3.17	13.64	2.04
Y-CG (in)	7.825	0.80	8.008	3.16	8.159	5.10	7.986	2.87
Mode 1 (Hz)	15.57	6.34	15.07	2.91	14.73	0.57	15.11	3.16
Mode 2 (Hz)	30.68	3.79	29.91	1.21	29.20	-1.21	29.82	0.88
Mode 3 (Hz)	82.44	-2.93	81.71	-3.79	82.63	-2.69	82.94	-2.34
Mode 5 (Hz)	178.3	-1.90	177.8	-2.16	179.1	-1.50	178.8	-1.64
Mode 6 (Hz)	203.0	-3.69	202.4	-3.95	205.4	-2.52	205.2	-2.62

[a] Modal Participation Factor.
Black shading: Objective function.
Gray shading: violated an approximate three- to five-percent requirement, active constraint, or too much error (for weight and CG locations).

Table 3. Auto- and cross-orthogonality matrices using baseline model.

Auto-orthogonality matrix						Cross-orthogonality matrix					
Mode	**1**	**2**	**3**	**5**	**6**	**Mode**	**1**	**2**	**3**	**5**	**6**
1	**1.000**	-0.431	-0.019	-0.110	0.143	1	**-0.867**	-0.287	0.007	0.038	0.016
2	-0.431	**1.000**	-0.491	0.775	0.382	2	-0.046	**0.798**	0.046	-0.080	0.003
3	-0.019	-0.491	**1.000**	-0.565	-0.405	3	0.218	-0.480	**-0.842**	0.055	-0.041
5	-0.110	0.775	-0.565	**1.000**	0.477	5	-0.226	0.773	0.111	**-0.534**	0.158
6	0.143	0.382	-0.405	0.477	**1.000**	6	-0.300	0.453	0.114	0.161	**0.816**

Gray shading: violate 10-percent (off-diagonal terms) and 90-percent (diagonal terms of COM) requirement.

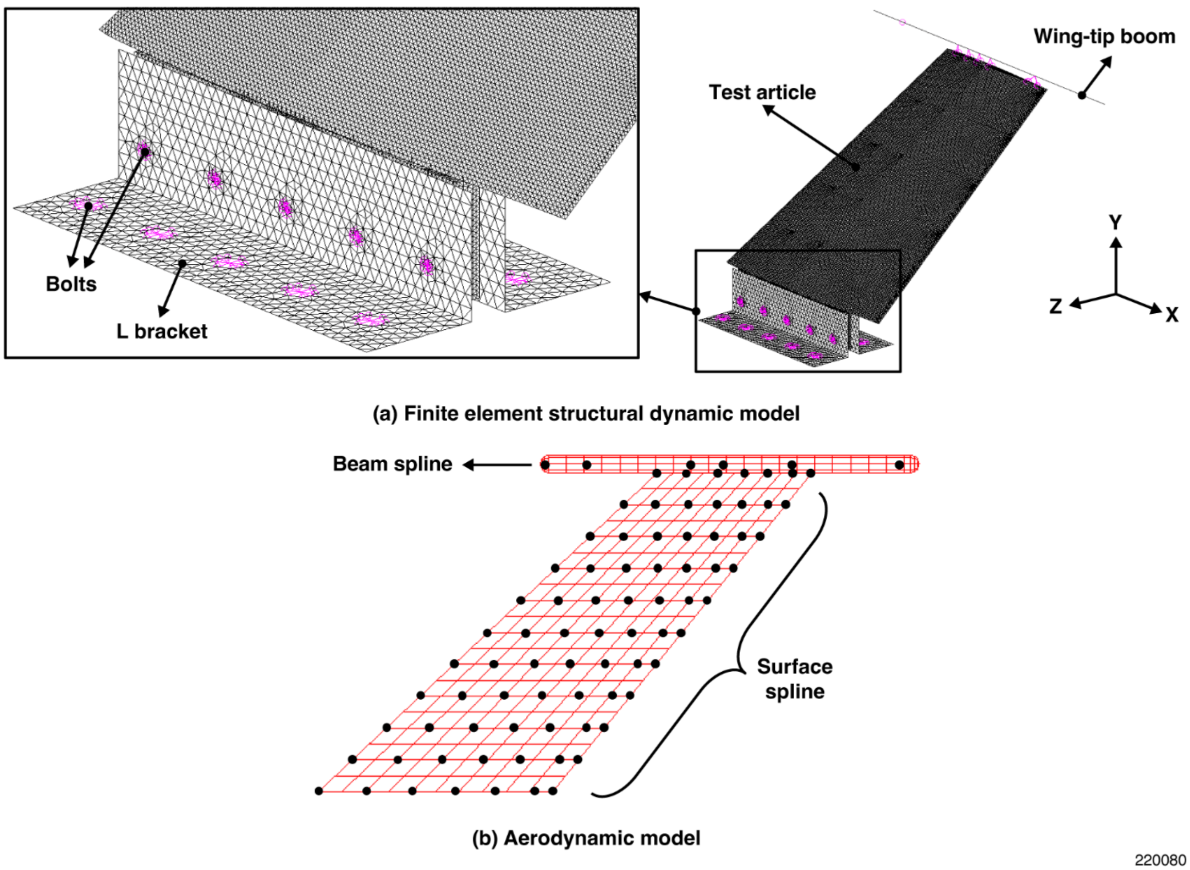

Figure 3. Structural and aerodynamic models of Aerostructure Test Wing IV.

Table 4. Flutter boundaries of Aerostructures Test Wing IV models.

Flutter boundary	Baseline model	Delivered model		Fixed model		After iteration 4	
		Value	% Difference	Value	% Difference	Value	% Difference
Speed (KEAS)	196.40	172.63	-12.1	177.43	-9.66	178.89	-8.91
Frequency (Hz)	29.92	25.85	-13.6	26.85	-10.3	25.93	-13.3

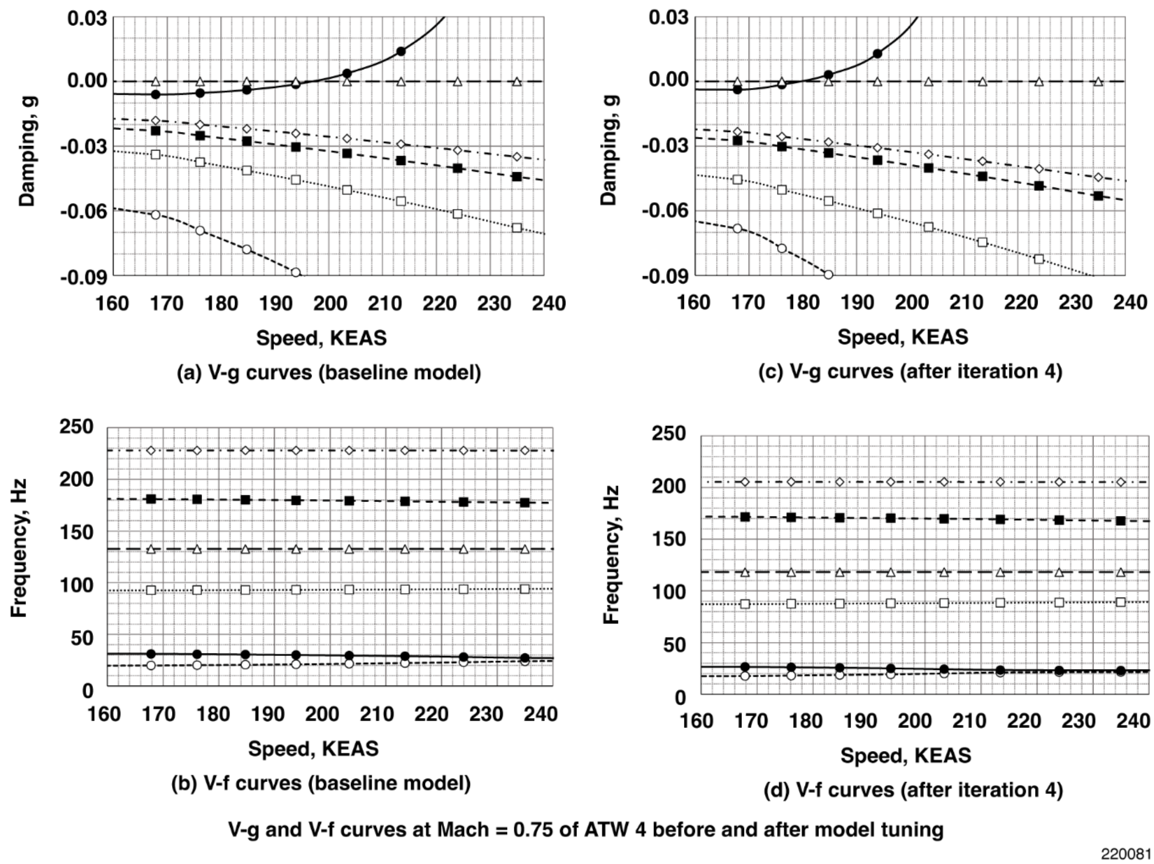

Figure 4. V-g and V-f curves at Mach 0.75 before and after model tuning.

Correlation of the Delivered Model

The STTR project team provided a tuned model, the "delivered model." This ATW IV FE model has uncertainties associated with the composite manufacturing process and the FE idealization used in the delivered model, which was already tuned by the contractor (ref. 18). The five natural frequencies, Modes (1, 2, 3, 5, and 6), of the delivered model are given in the top half section of table 2, sixth and seventh columns. The first two modes meet military and NASA requirements. The frequency errors for the third and fourth primary modes, however, violate the standards, and the frequency errors for the fifth mode (Mode 6) is relatively large. The corresponding AOM and COM are given in table 5. One off-diagonal term of the COM for the primary mode, 10.7 percent, violates "10-percent requirements" in military and NASA standards. This violation is negligibly small compared to the frequency violations.

Table 5. Auto- and cross-orthogonality matrices using delivered model.

Auto-orthogonality matrix						Cross-orthogonality matrix					
Mode	**1**	**2**	**3**	**5**	**6**	**Mode**	**1**	**2**	**3**	**5**	**6**
1	**1.000**	0.042	0.049	0.072	0.004	1	**0.998**	0.064	-0.024	-0.014	-0.003
2	0.042	**1.000**	-0.036	0.008	0.039	2	0.107	**-0.993**	0.034	0.030	-0.001
3	0.049	-0.036	**1.000**	0.093	0.007	3	0.024	0.004	**-0.999**	-0.022	0.005
5	0.072	0.008	0.093	**1.000**	0.031	5	0.061	-0.032	-0.070	**-0.933**	0.347
6	0.004	0.039	0.007	0.031	**1.000**	6	0.013	-0.029	-0.009	0.321	**0.946**

Gray shading: violate 10-percent requirement.

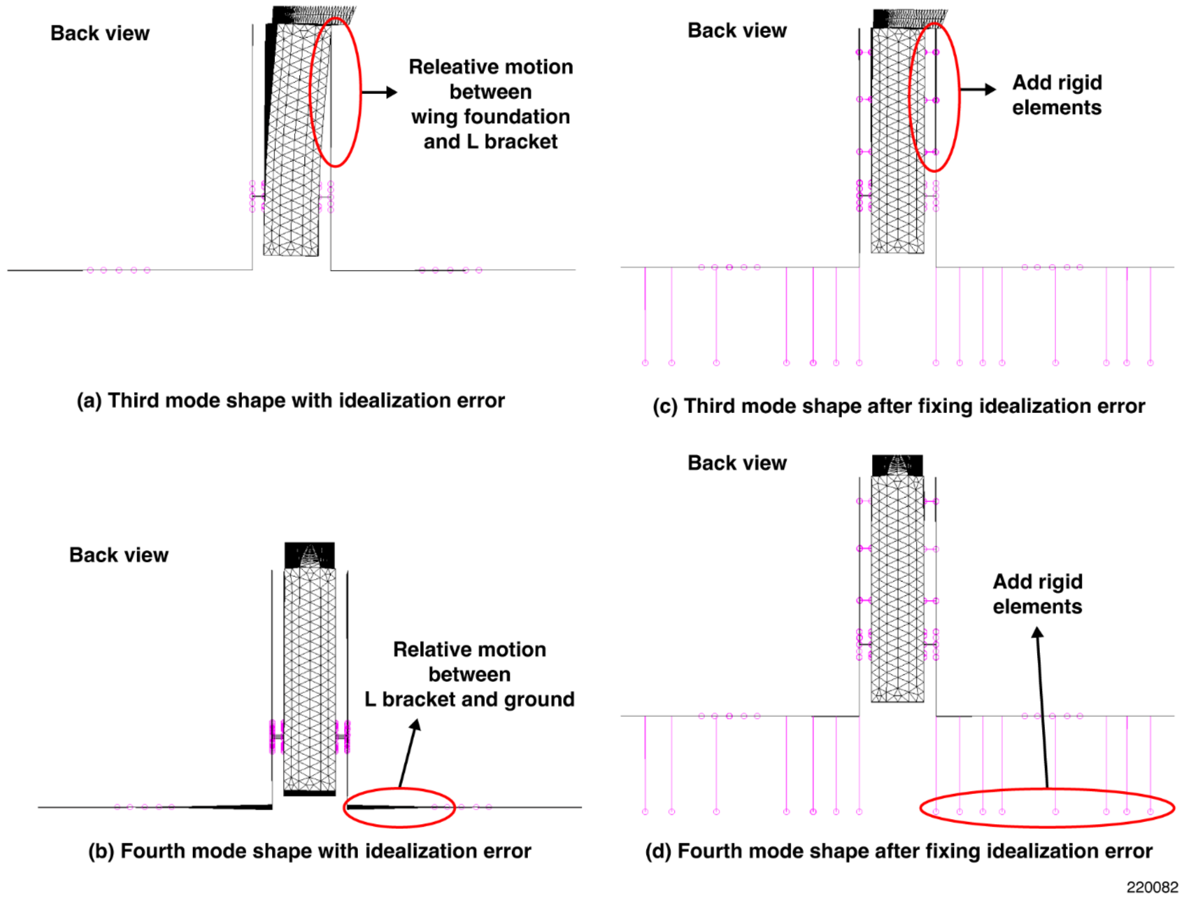

Figure 5. Relative motion between L-bracket and test article/ground.

Flutter analysis is performed using the delivered model, and the flutter speed and frequency are shown in table 4, third and fourth columns. The flutter speed and frequency differences are 12.1 and 13.6 percent, respectively. A huge improvement in the first two frequencies, AOM, and COM results in more than 12-percent flutter speed and frequency changes.

A composite test article is mounted on the ground using aluminum L-brackets and bolts, as shown in fig. 3(a). In the delivered model, these bolts are idealized as rigid and uniform beam elements (RBE2 and CBAR in NASTRAN terminology). As a result, the delivered FE model allows small relative motion between the L-brackets and the test article and the ground. The third and fourth mode shapes from the back view are prepared in fig. 5. Because of the relative motions shown in figs. 5(a) and 5(b), the corresponding frequencies are more flexible than the measured frequencies with huge prediction errors, 8.89 and 12.6 percent.

In this study, the FE model with the additional constraints at the L-bracket (fig. 6) will be called the "fixed model." An FE model with the candidate accelerometer DOF needs to be created to perform an efficient model tuning process. The candidate reduced-order models (ROMs) are shown in fig. 7.

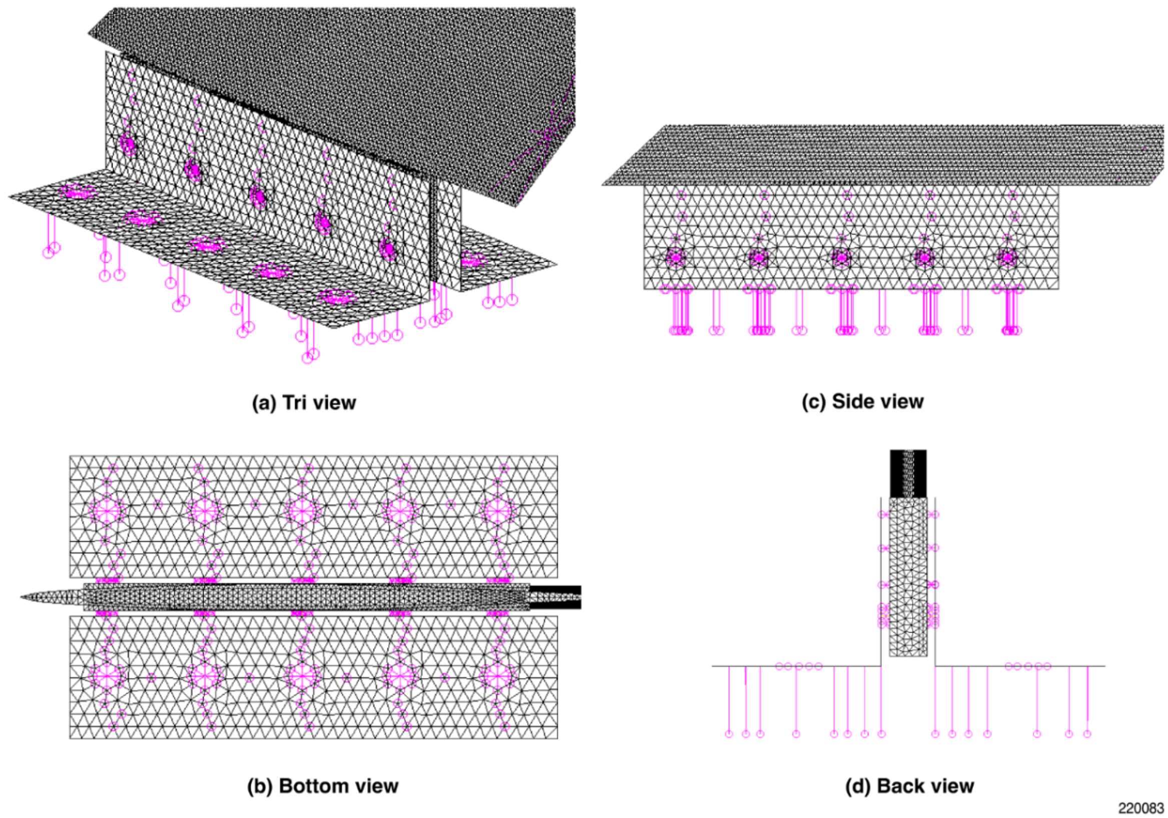

Figure 6. Additional constraints to minimize relative motion between L-bracket and test article/ground.

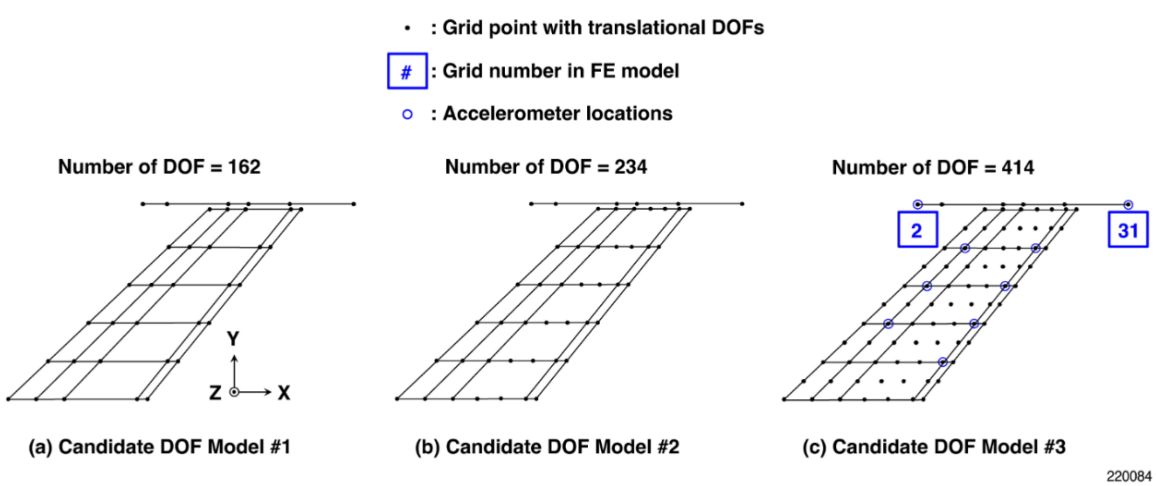

Figure 7. Finite element models with different numbers of candidate accelerometer degrees of freedom.

The first six natural frequencies from the FE models with the candidate accelerometer DOF (ASET cards using Guyan reduction) (ref. 16) are compared with the frequency results from the full-order model (FOM), as shown in table 6. This candidate accelerometer DOF is used as the reduced DOF for the model tuning. Corresponding mode shapes at grid numbers 2 and 31 (fig. 7) are given in table 7. In this study, ROM 3 (fig. 7(c)) is chosen from tables 6 and 7, and the maximum frequency and mode shape differences obtained from ROM 3 are less than one and 0.30 percent, respectively. The first five flexible modes, except the in-plane motion (Mode 4) from the fixed FOM are also summarized in the top half section of table 2, eighth and ninth columns. Figures 5(c) and 5(d) show the third and fourth mode shapes from the back view. Relative deformations in figs. 5(a) and 5(b) are suppressed using the additional rigid elements in fig. 6.

Table 6. Frequency comparisons with different degrees of freedom.

Mode number	FOM (438321)[a]	ROM[b] 1 (162)		ROM 2 (234)		ROM 3 (414)	
	Freq. (Hz)	Freq. (Hz)	% Error	Freq. (Hz)	% Error	Freq. (Hz)	% Error
1	15.17	15.17	0.00	15.17	0.00	15.17	0.00
2	30.08	30.08	0.00	30.08	0.00	30.08	0.00
3	81.01	81.37	0.46	81.16	0.19	81.12	0.14
4	119.1	119.2	0.01	119.2	0.01	119.1	0.01
5	175.3	177.0	0.99	176.4	0.66	176.1	0.46
6	198.8	206.0	**3.60**	202.1	**1.65**	200.6	**0.91**

[a]numbers in parentheses represents the number of degrees of freedom in the model.
[b]ROMs are based on Guyan reduction in NASTRAN.

Table 7. Mode shape comparisons with different degrees of freedom.

Mode number	Grid number	FOM (438321)	ROM 1 (162)		ROM 2 (234)		ROM 3 (414)	
		Shape	Shape	% Error	Shape	% Error	Shape	% Error
1	2 (Z)[a]	8.284	8.284	0.00	8.284	0.00	8.284	0.00
	31 (Z)	43.335	43.335	0.00	43.335	0.00	43.335	0.00
2	2 (Z)	50.055	50.055	0.00	50.055	0.00	50.055	0.00
	31 (Z)	-29.313	-29.313	0.00	-29.313	0.00	-29.313	0.00
3	2 (Z)	12.064	12.065	0.01	12.065	0.01	12.065	0.01
	31 (Z)	16.149	16.150	0.01	16.149	0.00	16.149	0.00
4	2 (X)[b]	18.268	18.268	0.00	18.268	0.00	18.268	0.00
	31 (X)	18.294	18.294	0.00	18.294	0.00	18.294	0.00
5	2 (Z)	9.412	9.393	-0.20	9.402	-0.10	9.408	-0.04
	31 (Z)	-7.453	-7.458	0.07	-7.453	-0.01	-7.453	-0.01
6	2 (Z)	9.535	9.628	**0.97**	9.579	**0.46**	9.557	**0.23**
	31 (Z)	11.261	11.333	0.64	11.282	0.18	11.274	0.11

(Z)[a] and (X)[b]: out of plane motion, and in plane motion (shown in figure 7, respectively).

When the idealization error is fixed, the frequency correlations are drastically improved, as shown in table 2. Mode 2 satisfies the military and NASA standards; moreover, the first, third, and fourth primary modes also satisfy the NASA standard. The frequency error for the secondary mode is also less than 10 percent. The AOM and COM are listed in table 8. Off-diagonal terms of the AOM and COM, 11 and 13 percent, violate the 10-percent requirement for primary modes.

Flutter analysis is also performed after fixing the idealization error, and the flutter speed and frequency results are given in table 4, fifth and sixth columns. Flutter speed improved more than 2.4 percent by correcting boundary condition problems with the delivered model. It should be noted that the idealization error can’t be improved with a model tuning procedure.

Table 8. Auto- and cross-orthogonality matrices using a fixed model.

Auto-orthogonality matrix						Cross-orthogonality matrix					
Mode	**1**	**2**	**3**	**5**	**6**	**Mode**	**1**	**2**	**3**	**5**	**6**
1	**1.000**	0.042	0.049	0.075	0.004	1	**0.999**	0.026	0.039	0.004	0.000
2	0.042	**1.000**	-0.037	0.020	0.032	2	0.069	**-0.997**	-0.011	-0.045	0.000
3	0.049	-0.037	**1.000**	0.110	-0.014	3	0.009	0.028	**0.999**	-0.028	0.023
5	0.075	0.020	0.110	**1.000**	0.080	5	0.067	-0.059	0.130	**0.932**	0.328
6	0.004	0.032	-0.014	0.080	**1.000**	6	0.007	-0.020	-0.042	-0.250	**0.967**

Gray shading: violate 10-percent requirement.

First Optimization Run

A total of 797 candidate design variables, as listed in table 9, are prepared in this study. These input cards for 797 design variables (DESVAR) (ref. 16) and design variable and model relations (such as DVMREL, DVPREL, and DVCREL) (ref. 16) must be included in the input deck of the NASTRAN solution 200. Once the sensitivity values of the response functions are obtained, the sensitivity values of the performance indices are computed using the in-house post-processing codes shown in fig.1. Absolute values of the objective sensitivity are sorted to select the most efficient design variables for optimizing the objective function value selected among performance indices. The total weight difference is nominated as an objective function value for the first optimization run without any constraint functions. A total of 25 of the most sensitive design variables in table 9 are selected for the first optimization run. The design variables for the first optimization run are the densities of material properties, the diameters of the wing-tip boom, and the composite plate thicknesses.

After the first optimization, a total weight of 1.744 lb becomes the target value 1.686 lb, as shown in bottom half of table 2, second and third columns; however, the first and second frequency errors of 3.55 and 1.79 percent become 6.34 and 3.79 percent, respectively. The AOM and COM in table 10 show a similar level of correlation with the fixed model as shown in table 8. It should be noted in table 2 that the X- and Y-CG location errors after the first optimization run are 1.32 and 0.80 percent, respectively, and these values are less than the 1.5-percent error.

Table 9. Design variables selected during optimization iterations.

Candidate DV #	Property (ref. 16)	Iteration 1	Iteration 2	Iteration 3	Iteration 4
1-15	MAT1	3	3	3	3
16-31	MAT8	2	2	2	2
32-34	PBARL	2	2	2	2
35	PSHELL				
36-120	CONM2		7	47	47
121-153	PELAS				
154-475	PCOMP (thickness)	18	50	80	80
476-797	PCOMP (ply angle)				
Total number of design variables		25	64	134	134

MAT1: the material properties for linear isotropic materials.
MAT8: the material properties for an orthotropic material for isoparametric shell elements.
PBARL: the properties of a simple beam element by cross-sectional dimensions.
PSHELL: the membrane, bending, transverse shear, and coupling properties of thin shell elements.
CONM2: a concentrated mass element at a grid point.
PELAS: the stiffness, damping coefficient, and stress coefficient of a scalar elastic (spring) elements.
PCOMP: the properties of an n-ply composite material laminate.

Second Optimization Run

The first frequency error is selected for the objective function of the second optimization run. In this case, total weight, X- and Y-CG locations, and frequency errors of the Modes (2, 3, 5, and 6) are chosen as the inequality constraint functions. The maximum allowable errors for the weight and frequency-related constraints are three and five percent, respectively. Before starting the second optimization run, sensitivity analysis with 797 design variables is again performed to decide the most efficient design variables. An additional 39 design variables, for a total of 64 (= 25 + 39) are selected, as shown in table 9, fourth column. The glue material used for bonding spars, ribs, and wing cover skins is not uniformly applied during the composite manufacturing process. Lumped mass properties (CONM2) for the glue material and balancing weight at the leading and trailing edges of the wing-tip boom are involved in the optimization run.

Table 10. Auto- and cross-orthogonality matrices after iteration one.

Auto-orthogonality Matrix						Cross-orthogonality Matrix					
Mode	**1**	**2**	**3**	**5**	**6**	**Mode**	**1**	**2**	**3**	**5**	**6**
1	**0.949**	0.035	0.058	0.072	0.002	1	**0.973**	0.024	-0.038	0.004	0.000
2	0.035	**0.960**	-0.033	0.018	0.030	2	0.06	**-0.977**	0.012	-0.045	0.000
3	0.058	-0.033	**0.968**	0.110	-0.015	3	0.021	0.024	**-0.982**	-0.029	-0.022
5	0.072	0.018	0.110	**0.975**	0.079	5	0.066	-0.058	-0.132	**0.92**	-0.323
6	0.002	0.030	-0.015	0.079	**0.977**	6	0.006	-0.019	0.044	-0.245	**-0.956**

Gray shading: violate 10-percent requirement.

The bottom half of table 2, fourth and fifth columns, show the first frequency error of 6.34 percent reduces to 2.91 percent after the second optimization run. It should be noted that the Y-CG location becomes an active constraint at 3.16 percent, and it may be concluded that the first frequency error can't be improved anymore because of the active constraint. The frequency errors for Modes (1, 2, and 5) are less than three percent. Similarly, frequency errors for Modes (3 and 6) are less than five percent. Table 11 shows that one of the off-diagonal terms of the primary modes of the AOM and COM is 11.3 and 13.3 percent, which slightly exceeds the 10-percent requirement.

Table 11. Auto- and cross-orthogonality matrices after iteration two.

Auto-orthogonality matrix						Cross-orthogonality matrix					
Mode	**1**	**2**	**3**	**5**	**6**	**Mode**	**1**	**2**	**3**	**5**	**6**
1	**1.062**	0.042	0.039	0.074	-0.004	1	**1.030**	0.027	0.040	-0.004	0.000
2	0.042	**1.051**	-0.043	0.025	0.029	2	0.067	**-1.022**	-0.011	0.046	0.000
3	0.039	-0.043	**1.016**	0.113	-0.013	3	-0.002	0.033	**1.006**	0.029	0.024
5	0.074	0.025	0.113	**1.005**	0.079	5	0.065	-0.063	0.133	**-0.934**	0.326
6	-0.004	0.029	-0.013	0.079	**1.002**	6	0.000	-0.017	-0.043	0.249	**0.969**

Gray shading: violate 10-percent requirement.

Third Optimization Run

The orthogonality of the AOM and COM is improved in this optimization run. The off-diagonal term of the AOM (11.3 percent) in table 11, fourth row (Mode 5), third column is selected as the objective function for the third optimization run. Based on the same sensitivity analysis procedure, 70 additional design variables are added, as shown in table 9 (fifth column).

In this optimization run, the total weight and X- and Y-CG locations belong to the inequality constraints with a maximum allowable error of five percent (compared to three percent in the second optimization run) to start optimization in a feasible domain (ref. 20). The maximum allowable frequency errors for Modes (1, 2), (5, 3), and (6) are 3, 5, and 10 percent, respectively. All off-diagonal terms of the AOM and COM are chosen as inequality constraints with a maximum allowable error of 10 percent, except for the objective function; the fourth row (Mode 5) and third column of the COM; the fifth row (Mode 6) and fourth column (Mode 5) elements of the COM; and the fourth row (Mode 5) and fifth column (Mode 6) elements of the COM. Based on the NASA standard, diagonal terms of the COM are also selected as inequality constraints. A minimum allowable error of 90 percent is used in the case of diagonal terms.

After the third optimization run, the objective function value becomes 7.6 percent (7.8 percent with normalization). The off-diagonal term for the third primary mode (13.3 percent in Table 11) also becomes less than 10 at 9.8 percent (9.9 percent with normalization), as shown in table 12. It should be noted in tables 10, 11, and 12 that the diagonal terms of the AOM are not equal to one because of the constant assumption for the expanded eigenmatrix Φ_{GR}, as shown in eq. (18). The bottom half of table 2, sixth and seventh columns shows frequency errors are all improved and satisfy inequality constraints. The inequality constraint associated with the Y-CG location, however, becomes an active constraint of 5.1 percent (slightly violating the 5-percent allowable).

Table 12. Auto- and cross-orthogonality matrices after iteration three.

Auto-orthogonality matrix						**Cross-orthogonality matrix**					
Mode	**1**	**2**	**3**	**5**	**6**	**Mode**	**1**	**2**	**3**	**5**	**6**
1	**1.038**	0.045	-0.001	0.068	0.029	1	**1.018**	0.026	0.040	-0.004	0.000
2	0.045	**1.044**	-0.054	0.040	0.041	2	0.071	**-1.018**	-0.008	0.044	0.000
3	-0.001	-0.054	**0.970**	**0.076**	-0.033	3	-0.041	0.044	**0.983**	0.024	0.026
5	0.068	0.040	**0.076**	**0.975**	0.075	5	0.061	-0.076	**0.098**	**-0.926**	0.315
6	0.029	0.041	-0.033	0.075	**0.957**	6	0.032	-0.027	-0.062	0.239	**0.946**

Black shading: Objective function
Yellow shading: not objective, nor constraint functions
Gray shading: secondary mode

Fourth Optimization Run

The Y-CG location error is selected as the objective function for the final optimization run with the same design variables as in table 9, sixth column. The same constraint functions used in the third optimization run are also used for the final optimization run. The objective function for the third optimization run becomes an additional constraint function (also including the fourth row and third column element of the COM) with a less than 10-percent limit.

Table 13. Auto- and cross-orthogonality matrices after iteration four.

Auto-orthogonality matrix						**Cross-orthogonality matrix**					
Mode	**1**	**2**	**3**	**5**	**6**	**Mode**	**1**	**2**	**3**	**5**	**6**
1	**1.000**	0.041	0.023	0.067	0.018	1	**0.999**	0.024	0.040	0.004	0.000
2	0.041	**1.000**	-0.044	0.030	0.036	2	0.066	**-0.997**	-0.009	-0.044	0.000
3	0.023	-0.044	**1.000**	0.081	-0.029	3	-0.017	0.035	**0.999**	-0.025	0.025
5	0.067	0.030	0.081	**1.000**	0.075	5	0.061	-0.069	0.099	**0.938**	0.320
6	0.018	0.036	-0.029	0.075	**1.000**	6	0.022	-0.023	-0.058	-0.247	**0.967**

Gray shading: secondary mode.

All results after the final optimization run are summarized in the bottom half of table 2, eighth and nineth columns, and table 13. All weight-related errors, including total weight, and X- and Y-CG locations are less than three percent. The most important primary frequency error - the second mode - is less than one percent. Similarly, the frequency errors of the other three primary modes are less than 3.2 percent, and the frequency error of the secondary mode (Mode 6) is less than 2.7 percent. The frequency errors of the first five out-of-plane modes are all less than 3.2 percent. After the final optimization run, the AOM is normalized; the AOM and COM are shown in table 13. Table 13 shows that all of the off-diagonal terms of the AOM are less than 10 percent. Similarly, all of the off-diagonal terms of the COM for the primary modes are less than 10 percent. Off-diagonal terms of the COM for the secondary mode become 24.7 and 32.0 percent. Also, of note, all diagonal terms of the COM are greater than 93.8 percent. The final FE model correlates well with the test data.

All of the design variables that change more than 5 percent after the final optimization run are summarized in table 14. The largest design variable change is a 12.7-percent decrease in the inner diameter of the circular wing-tip boom. This wing-tip boom is made with composite material, and the inner diameter of the hollow cross-sectional shape contains many uncertainties.

Flutter analysis is performed at the same Mach number again with the updated FE model to check the effect of the structural dynamic model tuning on the flutter boundary. After the final model tuning, the V-g and V-f curves are shown in figs. 4(c) and 4(d). Flutter speed and frequency are shown in table 4, seventh and eighth columns. Flutter speed and frequency improvements with respect to the baseline model are 8.91 and 13.3 percent, respectively. Roughly, 2.5 percent (= 12.1 – 9.66 percent) of this flutter speed improvement is a result of fixing the idealization error in the wing-root boundary condition.

Table 14. Design variables change more than five percent.

DV #	Property	% change	DV #	Property	% change	DV #	Property	% change
34	diameter	-12.7	115	CONM2	-6.33	371	PCOMP	-6.16
60	CONM2	-7.27	303	PCOMP	-6.17	372	PCOMP	-6.20
65	CONM2	6.22	304	PCOMP	-6.20	373	PCOMP	-6.16
108	CONM2	-5.16	305	PCOMP	-6.17	374	PCOMP	-7.24
109	CONM2	-6.89	306	PCOMP	-7.24	375	PCOMP	-7.23
110	CONM2	-7.98	307	PCOMP	-7.23	376	PCOMP	-7.24
111	CONM2	-8.83	308	PCOMP	-7.24	377	PCOMP	-5.20
112	CONM2	-8.78	309	PCOMP	-5.19	378	PCOMP	-5.10
113	CONM2	-8.08	310	PCOMP	-5.09	379	PCOMP	-5.21
114	CONM2	-7.57	311	PCOMP	-5.20			

CONM2: a concentrated mass element at a grid point.
PCOMP: the properties of an n-ply composite material laminate.

The total weight and frequencies of the fixed model in table 2 are already in acceptable shape. The average frequency error of the primary modes is 3.25 percent. After the four optimization iterations, the average frequency error becomes 2.01 percent; therefore, frequencies and total weight are improved by 1.24 and 2.26 percent, respectively. In table 4, the flutter speed improvement is 0.75 percent (= 9.66 – 8.91 percent); therefore, the 3-percent requirement (military standard) for the frequency correlation of the primary modes with 10-percent (11- and 13-percent) requirements for the off-diagonal terms of the AOM and COM is accurate enough to have a good flutter speed.

Finite Element Model Tuning of the Aerostructures Test Wing IV using Simulated Static Test Data

The static deformation module in fig. 1 is tested in this section. The computer simulated static data will be used.

Finite Element Model for a Simulated Static Test

The thicknesses of the aluminum L-bracket (0.25 in) and a single layer of a composite plate (0.005 in) are changed by five percent (0.2375 and 0.00525 in) to create a sample numerical test case. Structural deformations are computed at the deformation measurement points listed in table 15. Two load cases are considered in this model tuning with static deformation data. In the first case, one lb of positive Z-direction load is applied at one in, aft of the mid-chord of the wing-tip boom. On the other hand, one lb of negative Z-direction load is applied at the leading edge of the wing-tip boom in the second load case. Structural deformations under these two load cases are shown in fig. 8.

Table 15. Grid and degree of freedom information about deformation measurements

Deformation measurements number	Grid number with measured DOF
1	1847 (X)
2	2315 (Y)
3	1484 (Z)
4	1370 (Z)
5	2232 (X)
6	2606 (Y)
7	1754 (Z)

Model Tuning using Static Deformation Data

The objective function used in this test case is a linear combination of the performance indices for the first and second load cases given in eq. (31). Sensitivity values of the corresponding objective function value are shown in eq. (32):

Objective function $$J = J_{L1} + J_{L2} \tag{31}$$

Sensitivity of objective function $$\frac{\partial J}{\partial x_k} = \frac{\partial J_{L1}}{\partial x_k} + \frac{\partial J_{L2}}{\partial x_k} \tag{32}$$

where, J_{Li} $i = 1, 2$ are defined in equation (29).

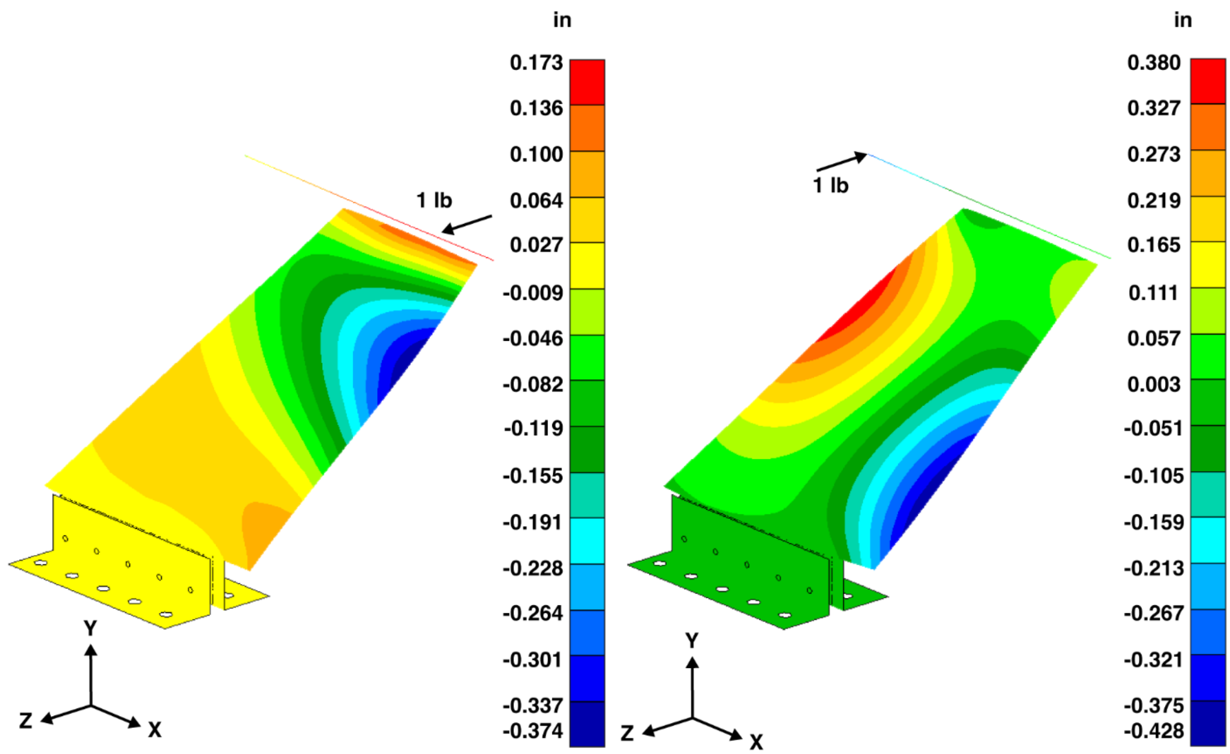

(a) Z deformation under load case 1

(b) Z deformation under load case 2

220085

Figure 8. Target deformation shapes under load cases one and two.

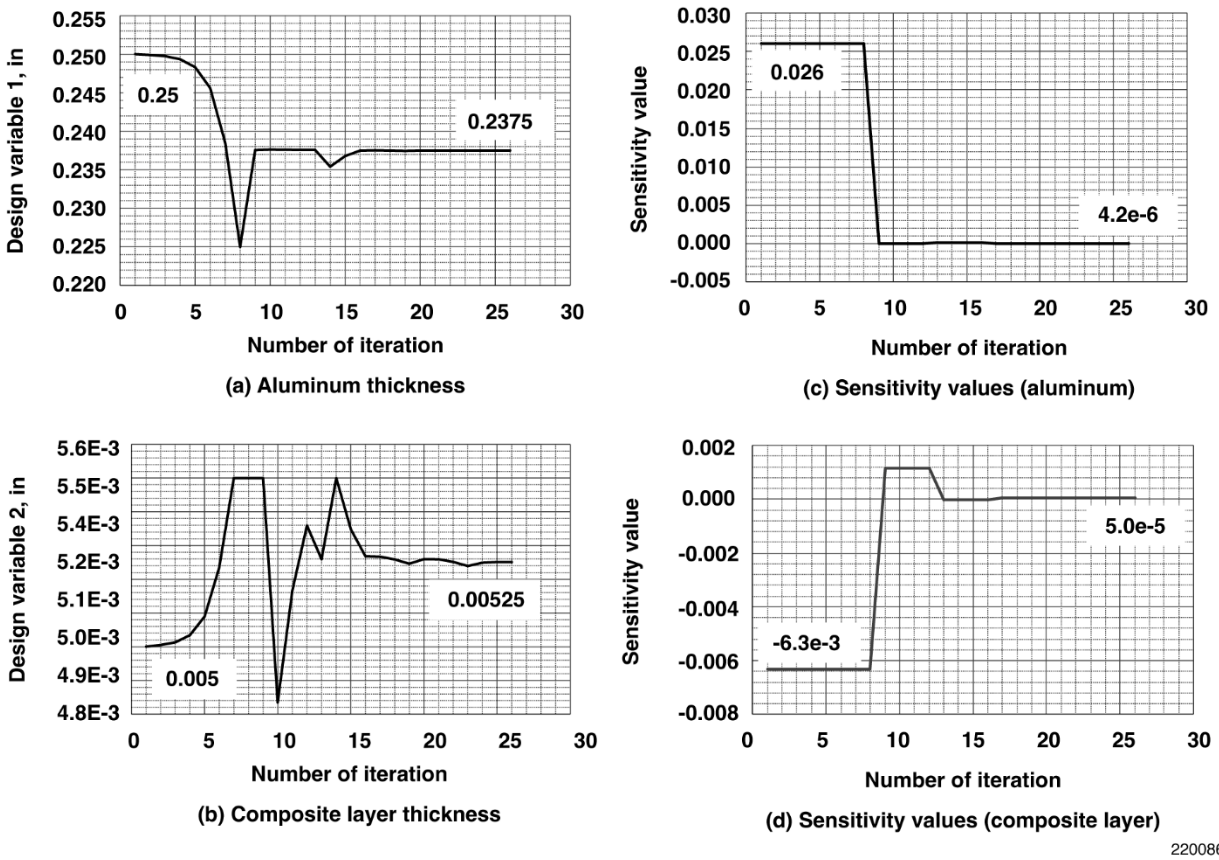

Figure 9. Histories of design variables and design variable sensitivities during an optimization run.

The histories of two design variables during the optimization run are shown in fig. 9. The initial starting values of design variables one and two are 0.25 and 0.005 in, respectively. Figures 9(c) and 9(d) show the sensitivity values of the objective function with respect to design variables one and two at the start of the optimization run are 0.026 and -0.0063, respectively. At the end of the optimization run, these sensitivity values become 4.2E-06 and 5.0E-05; therefore, the Kuhn-Tucker condition (ref. 20) is satisfied with an unconstrained optimization problem. After the optimization run, the design variables one and two become 0.2375 and 0.00525 in, respectively, as shown in figs. 9(a) and 9(b), which are target values used to generate target wing deformations in fig. 8. The performance of the static deformation module is demonstrated in this section.

Conclusions

This study introduced a structural model tuning tool based on analytical sensitivity values that has been developed. Analytical sensitivity values of performance indices are computed using the NASTRAN-generated sensitivity values with the in-house computer codes.

All of the analysis modules for the new structural model tuning tool are tested using the Aerostructures Test Wing IV, which was developed at the National Aeronautics and Space Administration Armstrong Flight Research Center using National Aeronautics and Space Administration Small Business Technology Transfer Phase II, NNX15CD08C, for demonstrating flutter and advanced aeroelastic test techniques. Structural dynamic and static model tunings are performed separately using measured ground vibration test data and computer simulated static data, respectively. The performance of the static deformation module has been demonstrated using the Aerostructures Test Wing IV model.

After the structural dynamic model tuning, all of the weight-related errors including total weight as well as X- and Y-CG locations are less than three percent. The frequency errors of the first five out-of-plane modes are all less than 3.2 percent. All of the off-diagonal terms of the auto-orthogonality matrix are less than 10 percent. Similarly, all of the off-diagonal terms of the cross-orthogonality matrix for the primary modes are less than 10 percent. Off-diagonal terms of the cross-orthogonality matrix for the secondary modes become 24.7 and 32.0 percent. All of the diagonal terms of the cross-orthogonality matrix are greater than 93.8 percent.

The final finite element model correlates well with the test data. The flutter speed decreases by 8.91 percent compared with the baseline Aerostructures Test Wing IV. Roughly, 2.5 percent of this flutter speed improvement is attributed to fixing the idealization error in the wing-root boundary condition. The 3-percent requirement for the frequency correlation of the primary modes with 10-percent requirements for the off-diagonal terms of the auto-orthogonality matrix and cross-orthogonality matrix is accurate enough to have a good flutter speed.

Appendix A: System Equivalent Reduction Expansion Process (ref. 17)

The governing equations of motion for an undamped structural system without any applied forces are written in eq. (A1):

$$\mathbf{M}\ddot{\boldsymbol{q}} + \mathbf{K}\boldsymbol{q} = \mathbf{0} \tag{A1}$$

where, $\mathbf{M}$ and $\mathbf{K}$ are the full-order mass and stiffness matrices, respectively; $\ddot{\boldsymbol{q}}$ and $\boldsymbol{q}$ are the acceleration and displacement vectors. The displacement vector $\boldsymbol{q}$ can be expressed using eigenmatrix $\boldsymbol{\Phi}$ and the generalized coordinate $\boldsymbol{\eta}$, as shown in eq. (A2):

$$\boldsymbol{q} = \boldsymbol{\Phi}\boldsymbol{\eta} \tag{A2}$$

Equations (A3) and (A4) show the displacement vector $\boldsymbol{q}$ and the eigenmatrix Φ can be partitioned:

$$\boldsymbol{q} = \begin{Bmatrix} \boldsymbol{q}_R \\ \boldsymbol{q}_O \end{Bmatrix} \tag{A3}$$

$$\boldsymbol{\Phi} = \begin{bmatrix} \boldsymbol{\Phi}_R \\ \boldsymbol{\Phi}_O \end{bmatrix} \tag{A4}$$

where, the '*R*' and '*O*' subscripts denote the reduced and omitted DOF, respectively. The reduced displacement vector $\boldsymbol{q}_R$, in eq. (A3); therefore, can be expressed in eq. (A5):

$$\boldsymbol{q}_R = \boldsymbol{\Phi}_R\boldsymbol{\eta} \tag{A5}$$

Multiplying $\boldsymbol{\Phi}_R^{\mathrm{T}}$ to eq. (A5) gives eq. (A6):

$$\boldsymbol{\Phi}_R^{\mathrm{T}}\boldsymbol{q}_R = \boldsymbol{\Phi}_R^{\mathrm{T}}\boldsymbol{\Phi}_R\boldsymbol{\eta} \tag{A6}$$

The generalized coordinate $\boldsymbol{\eta}$, therefore, becomes the eq. (A7):

$$\boldsymbol{\eta} = \left(\boldsymbol{\Phi}_R^{\mathrm{T}}\boldsymbol{\Phi}_R\right)^{-1}\boldsymbol{\Phi}_R^{\mathrm{T}}\boldsymbol{q}_R = \boldsymbol{\Psi}_R\boldsymbol{q}_R \tag{A7}$$

where, $\boldsymbol{\Psi}_R$ is obtained using a least-squares fitting in eq. (A8):

$$\boldsymbol{\Psi}_R = \left(\boldsymbol{\Phi}_R^{\mathrm{T}}\boldsymbol{\Phi}_R\right)^{-1}\boldsymbol{\Phi}_R^{\mathrm{T}} \tag{A8}$$

Substituting eq. (A7) into eq. (A2) gives eq. (A9); an order reduction based on a transformation matrix $\mathbf{T}$ is the System Equivalent Reduction Expansion Process.

$$\boldsymbol{q} = \boldsymbol{\Phi}\boldsymbol{\Psi}_R\boldsymbol{q}_R = \mathbf{T}\boldsymbol{q}_R \tag{A9}$$

Substituting the eq. (A9) into the governing equations of motion in eq. (A1) gives eq. (A10):

$$\mathbf{MT}\ddot{\boldsymbol{q}}_R + \mathbf{KT}\boldsymbol{q}_R = \mathbf{M}\boldsymbol{\Phi}\boldsymbol{\Psi}_R\ddot{\boldsymbol{q}}_R + \mathbf{K}\boldsymbol{\Phi}\boldsymbol{\Psi}_R\boldsymbol{q}_R = \mathbf{0} \tag{A10}$$

Multiplying $\boldsymbol{\Psi}_R^T\boldsymbol{\Phi}^{\mathrm{T}}$ to eq. (A10) gives the eq. (A11):

$$\boldsymbol{\Psi}_R^T\boldsymbol{\Phi}^{\mathrm{T}}\mathbf{M}\boldsymbol{\Phi}\boldsymbol{\Psi}_R\ddot{\boldsymbol{q}}_R + \boldsymbol{\Psi}_R^T\boldsymbol{\Phi}^{\mathrm{T}}\mathbf{K}\boldsymbol{\Phi}\boldsymbol{\Psi}_R\boldsymbol{q}_R = \mathbf{M}_R\ddot{\boldsymbol{q}}_R + \mathbf{K}_R\boldsymbol{q}_R = \mathbf{0} \tag{A11}$$

The reduced order mass, $\mathbf{M}_R$, and stiffness, $\mathbf{K}_R$, matrices; therefore, become eqs. (A12) and (A13), respectively:

$$\mathbf{M}_R = \boldsymbol{\Psi}_R^T\boldsymbol{\Phi}^{\mathrm{T}}\mathbf{M}\boldsymbol{\Phi}\boldsymbol{\Psi}_R = \boldsymbol{\Psi}_R^T\boldsymbol{\Psi}_R \tag{A12}$$

$$\mathbf{K}_R = \boldsymbol{\Psi}_R^T\boldsymbol{\Phi}^{\mathrm{T}}\mathbf{K}\boldsymbol{\Phi}\boldsymbol{\Psi}_R = \boldsymbol{\Psi}_R^T\left[\boldsymbol{\omega}_{\boldsymbol{n}}^{\mathbf{2}}\right]\boldsymbol{\Psi}_R \tag{A13}$$

Pre- and post-multiplying matrices $\boldsymbol{\Phi}_R^{\mathrm{T}}$ and $\boldsymbol{\Phi}_R$ to the reduced mass matrix $\mathbf{M}_R$, then gives eq. (A14):

$$\boldsymbol{\Phi}_R^{\mathrm{T}}\mathbf{M}_R\,\boldsymbol{\Phi}_R = \boldsymbol{\Phi}_R^{\mathrm{T}}\boldsymbol{\Psi}_R^T\boldsymbol{\Psi}_R\boldsymbol{\Phi}_R \tag{A14}$$

Substituting eq. (A8) into $\boldsymbol{\Psi}_R\boldsymbol{\Phi}_R$ in eq. (A14) gives eq. (A15):

$$\boldsymbol{\Psi}_R\boldsymbol{\Phi}_R = \left(\boldsymbol{\Phi}_R^{\mathrm{T}}\boldsymbol{\Phi}_R\right)^{-1}\boldsymbol{\Phi}_R^{\mathrm{T}}\boldsymbol{\Phi}_R = \boldsymbol{I} \tag{A15}$$

Equation (A14), therefore, becomes eq. (A16):

$$\boldsymbol{\Phi}_R^{\mathrm{T}}\mathbf{M}_R\,\boldsymbol{\Phi}_R = \boldsymbol{I} \tag{A16}$$

Similarly, eq. (A17) from eq. (A13):

$$\boldsymbol{\Phi}_R^{\mathrm{T}}\mathbf{K}_R\,\boldsymbol{\Phi}_R = \left[\boldsymbol{\omega}_{\boldsymbol{n}}^{\mathbf{2}}\right] \tag{A17}$$

The frequencies, therefore, from the ROM, $\mathbf{M}_R$ and $\mathbf{K}_R$, are identical with those from the full-order model. When the number of rows, n_{RDOF} of the eigenmatrix $\boldsymbol{\Phi}_R$, are greater than the number of columns (= number of modes m), then there will be zero frequency modes. The number of zero frequency modes will be $n_{RDOF} - m$.

Appendix B: Sensitivity of the matrix $\boldsymbol{\Psi_R} = \left(\boldsymbol{\Phi}_{\boldsymbol{R}}^{\mathbf{T}}\boldsymbol{\Phi}_{\boldsymbol{R}}\right)^{-\mathbf{1}}\boldsymbol{\Phi}_{\boldsymbol{R}}^{\mathbf{T}}$ with respect to design variable $\boldsymbol{x_k}$

The sensitivity of the matrix $\boldsymbol{\Psi}_R$ in eq. (B1) with respect to design variable x_k will be derived in this Appendix:

$$\boldsymbol{\Psi}_R = \left(\boldsymbol{\Phi}_R^{\mathrm{T}}\boldsymbol{\Phi}_R\right)^{-1}\boldsymbol{\Phi}_R^{\mathrm{T}} \tag{B1}$$

Multiply the matrix $\left(\boldsymbol{\Phi}_R^{\mathrm{T}}\boldsymbol{\Phi}_R\right)$ to both side of eq. (B1) gives eq. (B2):

$$\left(\boldsymbol{\Phi}_R^{\mathrm{T}}\boldsymbol{\Phi}_R\right)\boldsymbol{\Psi}_R = \boldsymbol{\Phi}_R^{\mathrm{T}} \tag{B2}$$

Taking the derivative of both sides of eq. (B2) with respect to the k-th design variable, x_k, gives eq. (B3):

$$\frac{\partial\left(\boldsymbol{\Phi}_R^{\mathrm{T}}\boldsymbol{\Phi}_R\right)\boldsymbol{\Psi}_R}{\partial x_k} = \frac{\partial\boldsymbol{\Phi}_R^{\mathrm{T}}}{\partial x_k} = \frac{\partial\left(\boldsymbol{\Phi}_R^{\mathrm{T}}\boldsymbol{\Phi}_R\right)}{\partial x_k}\boldsymbol{\Psi}_R + \left(\boldsymbol{\Phi}_R^{\mathrm{T}}\boldsymbol{\Phi}_R\right)\frac{\partial\boldsymbol{\Psi}_R}{\partial x_k} \tag{B3}$$

therefore, $\frac{\partial\boldsymbol{\Psi}_R}{\partial x_k}$ becomes eq. (B4):

$$\left(\boldsymbol{\Phi}_R^{\mathrm{T}}\boldsymbol{\Phi}_R\right)\frac{\partial\boldsymbol{\Psi}_R}{\partial x_k} = \frac{\partial\boldsymbol{\Phi}_R^{\mathrm{T}}}{\partial x_k} - \frac{\partial\left(\boldsymbol{\Phi}_R^{\mathrm{T}}\boldsymbol{\Phi}_R\right)}{\partial x_k}\boldsymbol{\Psi}_R = \frac{\partial\boldsymbol{\Phi}_R^{\mathrm{T}}}{\partial x_k} - \left(\frac{\partial\boldsymbol{\Phi}_R^{\mathrm{T}}}{\partial x_k}\boldsymbol{\Phi}_R + \boldsymbol{\Phi}_R^{\mathrm{T}}\frac{\partial\boldsymbol{\Phi}_R}{\partial x_k}\right)\boldsymbol{\Psi}_R \tag{B4}$$

Multiply the matrix $\left(\boldsymbol{\Phi}_R^{\mathrm{T}}\boldsymbol{\Phi}_R\right)^{-1}$ to both sides of eq. (B4) gives eq. (B5):

$$\frac{\partial\boldsymbol{\Psi}_R}{\partial x_k} = \left(\boldsymbol{\Phi}_R^{\mathrm{T}}\boldsymbol{\Phi}_R\right)^{-1}\frac{\partial\boldsymbol{\Phi}_R^{\mathrm{T}}}{\partial x_k} - \left(\boldsymbol{\Phi}_R^{\mathrm{T}}\boldsymbol{\Phi}_R\right)^{-1}\left(\frac{\partial\boldsymbol{\Phi}_R^{\mathrm{T}}}{\partial x_k}\boldsymbol{\Phi}_R + \boldsymbol{\Phi}_R^{\mathrm{T}}\frac{\partial\boldsymbol{\Phi}_R}{\partial x_k}\right)\left(\boldsymbol{\Phi}_R^{\mathrm{T}}\boldsymbol{\Phi}_R\right)^{-1}\boldsymbol{\Phi}_R^{\mathrm{T}} \tag{B5}$$

Appendix C: MSC NASTRAN Commands for Sensitivity Computation

The MSC NASTRAN[1] commands for sensitivity computations are summarized in this appendix.

Executive Control Commands

ASSIGN: Assigns Physical File.

Assigns ASCII files that are used by post-processors.

Format:
assign userfile='filename', unit=#, status=unknown, form=formatted

Example:
assign userfile='results.csv', unit=52, status=unknown, form=formatted

Case Control Commands

DESVAR: Design Variable Selection.

Selects a set of DESVAR entries for the design set to be used.

Format:

DESVAR = [	ALL n	]

Example:
DESVAR=ALL

Describer	Meaning
n	Set identification of a previously appearing SET command (Integer > 0). Only DESVAR Case Control commands with IDs that appear on this SET command will be used in the SOL 200 design task.

Remarks:

1. Only one DESVAR Case Control command may appear in the Case Control Section and should appear above all subcase commands.
2. The DESVAR Case Control command is optional. If it is absent, all DESVAR Bulk Data entries will be used.

DSAPRT: Design Sensitivity Output Parameters

Specifies design sensitivity output parameters.

Format:

DSAPRT [	FORMATTED [UNFORMATTED],	[NOEXPORT], EXPORT	START=i,	BY=j,	END=k]	=	ALL [n]

[1] MSC NASTRAN 2018 Quick Reference Guide, MacNeal-Schwendler Corp., Newport Beach, CA, 2017.

NOPRINT	NONE

Example:
DSAPRT(FORMATTED, END=SENS)=ALL

Describer	Meaning
FORMATTED	Output will be presented with headings and labels.
UNFORMATTED	Output will be printed as a matrix print (see description of the MATPRN module in the MSC NASTRAN DMAP Programmer's Guide).
NOPRINT	No output will be printed.
EXPORT	Output will be exported to an external binary file specified by PARAM, IUNIT.
NOEXPORT	Output will not be exported to an external binary file.
START=i	Specifies the first design cycle for output (Integer > 0 or Character: "FIRST" or "LAST"; Default = 1 or "FIRST").
BY=j	Specifies the design cycle interval for output. See Remark 2 (Integer > 0; Default = 0).
END=k	Specifies the last design cycle for output (Integer > 0 or Character: "FIRST," "LAST," or "SENS;" Default = "LAST").
ALL	All retained design responses (defined on DRESP1, DRESP2 and DRESP3 entries) will be output.
n	Set identification of a previously appearing SET command. Only sensitivities of retained responses with identification numbers that appear on this SET command will be output (Integer > 0).

Remarks:

1. Only one DSAPRT may appear in the Case Control Section and it must occur with or above the first SUBCASE command.
2. Sensitivity data will be output at design cycles i, i+j, i+2j, ..., k. Note that the BY=0 implies no sensitivity results will be output at the intermediate design cycles.
3. <u>END=SENS requests design sensitivity analysis, and no optimization will be performed.</u>
4. If both DSAPRT and PARAM, OPTEXIT, 4, -4, or 7 are specified, then DSAPRT overrides PARAM, OPTEXIT, 4, -4, or 7. PARAM, OPTEXIT values and the equivalent DSAPRT commands are described as follows:

OPTEXIT	Equivalent DSAPRT Command
4	DSAPRT(UNFORMATTED, END=SENS)
-4	DSAPRT(NOPRINT, EXPORT, END=SENS)
7	DSAPRT(UNFORMATTED, START=LAST)

5. The n and NONE options are not supported for UNFORMATTED output. Only the UNFORMATTED option is supported for EXPORT.
6. PARAM, DSZERO can be used to set a threshold for the absolute value of the formatted sensitivity prints.
7. Design Sensitivity analysis is never performed following a discrete design optimization; therefore, no sensitivity output will be produced with DSAPRT(END=LAST) when discrete optimization is performed at the end of a job.
8. Formatted sensitivity data can also be written into Comma Separated Values (or CSV) file with following steps
    a. DSAPRT (formatted, …) request in case control. Note that "formatted" is a default option.
    b. PARAM, XYUNIT, 52 in bulk data. Unit 52 is simply chosen as an example.
    c. file assignment statement, such as:
    ASSIGN USERFILE='jobname.csv' FORM=formatted STATUS=new UNIT=52

DESOBJ: Design Objective

Selects the DRESP1, DRESP2, or DRESP3 entry to be used as the design objective.

Format:
DESOBJ [(MAX MIN)] = n
Example:
DESOBJ(MIN) = 200

Describer	Meaning
MIN	Specifies that the objective is to be minimized.
MAX	Specifies that the objective is to be maximized.
n	Set identification number of a DRESP1, DRESP2, or DRESP3 Bulk Data entry (Integer > 0).

Remarks:
1. A DESOBJ command is required for a design optimization task and is optional for a sensitivity task. Only one DESOBJ command may appear in a Case Control Section.
2. The referenced DRESPi entry must define a scalar response (e.g., WEIGHT or VOLUME). DRESPi is a “response quantity”
3. If the DESOBJ command refers to a global response, such as weight, it should appear above the first subcase. If the DESOBJ command refers to a subcase-dependent response such as an element stress, it should appear in that subcase. If it refers to a subcase dependent response but is inserted above the first subcase, it will select the response from the first subcase for the objective and ignore the responses in subsequent subcases.
4. Using DREPS2 with weight factors, SOL200 can support multiple objective optimizations.
5. MSC.NASTRAN MultiOpt utility supports Multi Model Optimization (MMO) and Global Optimization (GO), see Design Sensitivity and Optimization User’s Guide

DESSUB: Design Constraints Request at the Subcase Level

Selects the design constraints to be used in a design optimization task for the current subcase.

Format:
DESSUB = n
Example:
DESSUB = 2000

Describer	Meaning
n	Set identification of a set of DCONSTR / a DCONADD Bulk Data entry identification number (Integer > 0).

Remarks:
1. A DESSUB Case Control command is required for every subcase for which constraints are to be applied. An exception to this is “global constraints,” which are selected by the DESGLB Case Control command.
2. All DCONSTR and DCONADD Bulk Data entries with the selected set ID will be used.
3. Constraints cannot be applied to the FRMASS, FATIGUE, or FRFTG response using the DESSSUB command [B1]. Use the DESGLB command instead.

Bulk Data Commands

DESVAR: Design Variable

Defines a design variable for design optimization.

Format:

1	2	3	4	5	6	7	8	9	
DESVAR	ID	LABEL	XINIT	XLB	XUB	DELXV	DDVAL		

Example:

DESVAR	43	DV043	0.1	-2.0	2.0				

Describer	Meaning
ID	Unique design variable identification number. (Integer > 0)
LABEL	User-supplied name for printing purposes. (Character)
XINIT	Initial value. (Real; XLB < XINIT < XUB)
XLB	Lower bound. (Real; Default = -1.0E+20)
XUB	Upper bound. (Real; Default = +1.0E+20)
DELXV	Fractional change allowed for the design variable during approximate optimization. (Real > 0.0; for Default see Remark 2.)
DDVAL	ID of a DDVAL entry that provides a set of allowable discrete values. (Blank or Integer > 0; Default=blank for continuous design variables. See Remark 3.)

Remarks:

1. DELXV can be used to control the change in the design variable during one optimization cycle.
2. If DELXV is blank, the default is taken from the specification of the DELX parameter on the DOPTPRM entry. If DELX is not specified, then the default is 0.5.
3. If the design variable is to be discrete (Integer > 0 in DDVAL field), and if either of the XLB and/or XUB bounds are wider than those given by the discrete list of values on the corresponding DDVAL entry, XLB and/or XUB will be replaced by the minimum and maximum discrete values.

DVCREL1: Design Variable to Connectivity Property Relation

Defines the relation between a connectivity property and design variables.

Format:

1	2	3	4	5	6	7	8	9	
DVCREL1	ID	TYPE	EID	CPNAME	CPMIN	CPMAX	C0		
	DVID1	COEF1	DVID2	COEF2	DVID3	COEF3	Etc.		

Example:

DVCREL1	7	CONM2	41	X2					+
+	47	1.0							

Describer	Meaning
ID	Unique identification number (Integer > 0).
TYPE	Name of an element connectivity entry, such as "CBAR," "CQUAD4," etcetera (Character).
EID	Element Identification number (Integer > 0).
CPNAME	Name of connectivity property such as "X1," "X2," "X3," "ZOFFS," etcetera (**Character**).
CPMIN	Minimum value allowed for this property. If CPNAME references a connectivity property that can only be positive, then the default value of CPMIN is 1.0E-15. Otherwise, it is -1.0E35. See Remark 4 (Real).
CPMAX	Maximum value allowed for this property. See Remark 4 (Real; Default =1.0E+20).
C0	Constant term of relation (Real; Default = 0.0).
DVIDi	DESVAR entry identification number (Integer > 0).
COEFi	Coefficient of linear relation or keyword = "PVAL". See Remark 7 (If i = 1, Real or Character; if i > 1, Real).

Remarks:

1. The relationship between the connectivity property and design variables is given by: $CP_j = C_0 + \sum_i COEF_i \times x_{DVID_i}$.
2. The continuation entry is required.
3. The fifth field of the entry "CPNAME" only accepts string characters. These string values must be the same as those given in the connectivity entry descriptions in this guide. For example, if the plate offset is to be designed (CQUAD4, CTRIA3, etcetera), ZOFFS (case insensitive) must be specified on the CPNAME field.
4. The default values for "CPMIN" and "CPMAX" are not applied when the linear property is a function of a single design variable and C0=0. It is expected that the limits applied on the associated DESVAR entry will keep the designed property within meaningful bounds.
5. When "PVAL" is used for the COEF1 field, this is a flag to indicate that the COEF1 value is to be obtained from the connectivity bulk data entry. If a DVCREL1 entry references more than one design variable with the PVAL option, a "User Fatal" message will be issued
6. If the user inputs CQUAD4/CTRIA3 entries and then uses QRMETH = 5 to convert them to CQUADR/CTRIAR entries, the design of items on these entries using the DVCREL1 entry should refer to the converted type (i.e., CQUADR/CTRIAR). Similarly, if QRMETH=2 or 3 is used, the DVCREL1 entry should refer to CQUAD4/CTRIA3 types.

DVMREL1: Design Variable to Material Relation

Defines the relation between a material property and design variables.

Format:

1	2	3	4	5	6	7	8	9	
DVMREL1	ID	TYPE	MID	MPNAME	MPMIN	MPMAX	C0		
	DVID1	COEF1	DVID2	COEF2	DVID3	COEF3	Etc.		

Example:

DVMREL1	1	MAT1	301	E					+
+	1	1.0							
DVMREL1	19	MAT8	201	RHO					+
+	19	1.0							

Describer	Meaning
ID	Unique identification number. (Integer > 0)
TYPE	Name of a property entry, such as “MAT1”, “MAT2”, etc. (Character)
MID	Material identification number. (Integer > 0)
MPNAME	Name of material property, such as “E” or “RHO”. (Character)
MPMIN	Minimum value allowed for this property. If MPNAME references a material property that can only be positive, then the default value for MPMIN is 1.0E-15. Otherwise, it is -1.0E35. See Remark 4 (Real).
MPMAX	Maximum value allowed for this property. See Remark 4. (Real; Default = 1.0E+20)
C0	Constant term of relation (Real; Default = 0.0).
DVIDi	DESVAR entry identification number (Integer > 0).
COEFi	Coefficient of linear relation or keyword = “PVAL” (if i = 1, Real or Character; if i > 1, Real).

Remarks:

1. The relationship between the material property and design variables is given by: $MP_j = C_0 + \sum_i COEF_i \times x_{DVID_i}$.
2. The continuation entry is required.
3. The fifth field of the entry “MPNAME” only accepts string characters. It must be the same as the name that appears in the Bulk Data Entries for various material properties. For example, if the isotropic material density is to be designed, RHO (case insensitive) must be specified on the MPNAME field.
4. The default value for “MPMIN” and “MPMAX” are not applied when the linear property is a function of a single design variable and C0=0.0. It is expected that the limits applied to the DESVAR entry will keep the designed property within reasonable bounds.
5. When "PVAL" is used for the COEF1 field, this is a flag to indicate that the COEF1 value is to be obtained from the material bulk data entry. If a DVMREL1 entry references more than one design variable with the PVAL option, a User Fatal message will be issued.

DVPREL1: Design Variable to Property Relation

Defines the relation between an analysis model property and design variables.

Format:

1	2	3	4	5	6	7	8	9	
DVPREL1	ID	TYPE	PID	PNAME/FID	PMIN	PMAX	C0		
	DVID1	COEF1	DVID2	COEF2	DVID3	COEF3	Etc.		

Example:

DVPREL1	4	PBAR	1	7					+
+	4	1.0							

Describer	Meaning
ID	Unique identification number. (Integer > 0)
TYPE	Name of a property entry, such as “PBAR”, “PBEAM”, “PSHELL”, etc. (Character)
PID	Property entry identification number. (Integer > 0)
PNAME/FID	Property name, such as “T”, “A”, or field position of the property entry, or word position in the element property table of the analysis model. Property names that begin with an integer such as 12I/T**3 may only be referred to by field position. (Character or Integer 0)
PMIN	Minimum value allowed for this property. If PMIN references a property that can only be positive, then the default value for PMIN is 1.0E-15. Otherwise, it is -1.0E35. See Remark 6. (Real)
PMAX	Maximum value allowed for this property. (Real; Default = 1.0E+20)
C0	Constant term of relation. (Real; Default = 0.0)
DVIDi	DESVAR entry identification number. (Integer > 0)
COEFi	Coefficient of linear relation or keyword = “PVAL”. See Remark 7. (If i = 1, Real or Character; if i > 1, Real)

Remarks:

3. The relationship between the analysis model property and design variables is given by: $P_j = C_0 + \sum_i COEF_i \times x_{DVID_i}$.
4. The continuation entry is required.
5. TYPE = “PBEND” is not supported. TYPE = “PBEAML” supports only PNAME and not FID.
6. FID may be either a positive or a negative number. If FID > 0, it identifies the field position on a property entry. If FID < 0, it identifies the word position of an entry in the element property table. For example, to specify the area of a PBAR, either PNAME=A, FID=+4, or FID = -3 can be used. In general, use of PNAME is recommended. For Type "PBUSH," PNAME is recommended, if FID is used it must be < 0.
7. Designing “PBEAML” or “PBEAM” requires specification of both property name and station. Table C1 shows several examples.

Table C1

PTYPE	Property Name	END A	END B	i-th Station
PBEAML	DIM1	DIM1 or DIM1(A)	DIM1(B)	DIM1(i)
PBEAM	A	A or A(A)	A(B)	A(i)

Only stations that are input on a PBEAM or PBEAML entry can be referenced by a DVPREL1. For example, referencing an END B property name on a DVPREL1 entry when the referenced PBEAM does not explicitly specify the END B station, is not allowed.

8. The default values of PMIN and PMAX are not applied when the linear property is a function of a single design variable and C0=0. It is expected that the limits applied on the DESVAR entry will keep the designed property within reasonable bounds.
9. Please refer to the NASTRAN manual for more remarks.

DRESP1: Design Sensitivity Response Quantities

Defines a set of structural responses that are used in the design either as constraints or as an objective.

Format:

1	2	3	4	5	6	7	8	9	
DRESP1	ID	LABEL	RTYPE	PTYPE	REGION	ATTA	ATTB	ATT1	
	ATT2								

Example:

DRESP1	302	FREQ2	FREQ			2			
DRESP1	401	SHAPE1	DISP			123456	1	2	+
+	3								
DRESP1	204	W44	Weight			4	4		

Describer	Meaning
ID	Unique entry identifier (Integer > 0).
LABEL	User-defined label (Character).
RTYPE	Response type. See Table C2. (Character)
PTYPE	Element flag (PTYPE = “ELEM”) or property entry name. Used with element type responses (stress, strain, force, etcetera) to identify the property type, since property entry IDs are not unique across property types (Character: “ELEM,” “PBAR,” “PSHELL,” etcetera).
REGION	Region identifier for constraint screening. See footnote[1] for defaults (Integer > 0).
ATTA, ATTB, ATTi	Response attributes. See table C2 (Integer > 0, Real, or Blank).

Table C2. Design Sensitivity Response Attributes.

Response Type (RTYPE)	**ATTA (Integer > 0)**	**ATTB (Integer > 0 or Real > 0.0)**	**Atti (Integer > 0)**
WEIGHT	Row Number (1 < ROW < 6) See Remark 24	Column Number (1 < COL < 6)	SEIDi or ALL or blank. See Remark 12
FREQ	Normal Modes Mode Number. See Remarks 18 and 33	Approximation Code. See Remark 19.	Blank
DISP	Displacement Component (**should be ASET DOF**)		Grid ID

Remarks:

7. If RTYPE = “DISP,” “SPCFORCE,” “GPFORCE,” “TDISP,” “TVELO,” “TACCL,” or “TSPCF,” multiple component numbers (any unique combination of the digits 1 through 6 **with no embedded blanks**) may be specified on a single entry. Multiple response components may not be used on any other response types
12. If RTYPE = “WEIGHT,” “VOLUME,” or “TOTSE;” field **ATTi = “ALL” implies total weight**/volume/total strain energy of all superelements except external superelements; 0 implies residual only; and i implies SEID=i. Default = “ALL.” RTYPE = “TOTSE” is not supported for shape optimization.
18. RTYPE = “EIGN” refers to a normal modes response in terms of eigenvalue. (radian/time)**2, while RTYPE = “FREQ” refers to normal modes response in terms of natural frequency or units of cycles per unit time.

19. For RTYPE = LAMA, EIGN, or FREQ, the response approximation used for optimization can be individually selected using the ATTB field when APRCOD = 1 is being used.
    For RTYPE = LAMA, ATTB = blank or 1 selects direct linearization, ATTB = 2 = inverse linearization.
    For RTYPE = EIGEN or FREQ, ATTB = blank = Rayleigh Quotient Approximation, = 1 = direct linearization, = 2 = inverse approximation. The default Rayleigh Quotient Approximation should be preferred in most cases.
24. Design response weight is obtained from Grid Point Weight Generator for a reference point GRDPNT (see parameter GRDPNT). If GRDPNT is either not defined, equal to zero, or not a defined grid point, the reference point is taken as the origin of the basic coordinate system. Fields ATTA and ATTB refer to the row and column numbers of the rigid body weight matrix, which is partitioned as follows:

$$[W] = \begin{bmatrix} W_x & W_{12} & W_{13} & W_{14} & W_{15} & W_{16} \\ W_{21} & W_y & W_{23} & W_{24} & W_{25} & W_{26} \\ W_{31} & W_{32} & W_z & W_{34} & W_{35} & W_{36} \\ W_{41} & W_{42} & W_{43} & I_x & W_{45} & W_{46} \\ W_{51} & W_{52} & W_{53} & W_{54} & I_y & W_{56} \\ W_{61} & W_{62} & W_{63} & W_{64} & W_{65} & I_z \end{bmatrix}$$

    The default values of ATTA and ATTB are 3, which specifies weight in the Z direction. Field ATT1 = “ALL” implies total weight of all superelements except external superelements. SEIDi refers to a superelement identification number. SEIDi = “0” refers to the residual superelement. The default of ATT1 is blank which is equivalent to “ALL”
33. For RTYPE=EIGN or FREQ, PTYPE field can be utilized to identify the source of the mode. Valid options are “STRUC” or “FLUID.” The default is “STRUC.”

DRESP2: Design Sensitivity Equation Response Quantities

Defines equation responses that are used in the design, either as constraints or as an objective.

Format:

1	2	3	4	5	6	7	8	9	
DRESP2	ID	Label	EQID or FUNC	Region	Method	C1	C2	C3	
	“DRESP1”	NR1	NR2	NR3	NR4	NR5	NR6	NR7	
		NR8	Etc.						
	“DRESP2”	NRR1	NRR2	NRR3	NRR4	NRR5	NRR6	NRR7	
		NRR8	Etc.						

Example:

DRESP2	211	Xcg	901						+
+	DRESP1	201	200						
DRESP2	214	Ixx	902						+
+	DRESP1	204	200						+
+	DRESP2	212	213						
DRESP2	215	Iyx	903						+
+	DRESP1	205	200						+
+	DRESP2	212	211						

Describer	Meaning
ID	Unique entry identifier (Integer > 0).
Label	User-defined label (Character).
EQID	DEQATN entry identification number (Integer > 0).
FUNC	Function to be applied to the arguments. Refer [5] (Character).
Region	Region identifier for constraint screening. See Remark 5 (Integer > 0).
Method	When used with FUNC = BETA, METHOD = MIN indicates a minimization task, while MAX indicates a maximization task. (Default = MIN) when used with FUNCT = MATCH, METHOD = LS indicated a least squares, while METHOD = BETA indicated minimization of the maximum difference (Default = LS).
Ci	Constants used when FUNC = BETA or FUNC = MATCH in combination with METHOD = BETA. See Remark 8. (Real; Defaults: C1 = 1.0., C2 = .005, and C3=10.0)
“DRESP1”	Flag indicating DRESP1 entry identification numbers (Character). See Remark 13.
NRk	DRESP1 entry identification number (Integer > 0).
“DRESP2”	Flag indicating other DRESP2 entry identification number (Character). See Remark 13.
NRRk	DRESP2 entry identification number (Integer > 0).

Remarks:

5. The “REGION” field follows the same rules as for the DRESP1 entries. DRESP1 and DRESP2 responses will never be contained in the same region, even if they are assigned the same REGION identification number. The default is to put all responses referenced by one DRESP2 entry in the same region.
13. If the mathematical function from a DRESP1 that has character input in the ATTB field (see remark 20 of the DRESP1) is to be used in the DRESP2 evaluation, the DRESP1 must be referenced under the "DRESP2" flag, not the "DRESP1" flag. If the "DRESP1" flag is used in this situation, it will result in a DRESP2 being evaluated for each of the individual values that contribute to the mathematical function.

DEQATN: Equation Definition

Defines one or more equations for use in analysis.

Format:

1	2	3	4	5	6	7	8	9	
DEQATN	EQID	EQUATION							
	EQUATION (continued)								

Example:

DEQATN	901	F(R1,R2) = R1/R2	
DEQATN	902	F(R1,R2,R3,R4) = R1-R2*(R3**2+R4**2)	
DEQATN	903	F(R1,R2,R3,R4) = -R1-R2*R3*R4	

Describer	Meaning
EQID	Unique equation identification number (Integer > 0).
EQUATION	Equation(s). See Remarks (Character).

Remarks: Refer to MSC NASTRAN manual[1]

DSCREEN: Design Constraint Screening Data

Defines screening data for constraint deletion.

Format:

1	2	3	4	5	6	7	8	9	
DSCREEN	RTYPE	TRS	NSTR						

Example:

DSCREEN	DISP		500			2			

Describer	Meaning
RTYPE	Response type for which the screening criteria apply. See Remark 3 (Character).
TRS	Truncation threshold (Real; Default = -0.5).
NSTR	Maximum number of constraints to be retained per region per load case. See Remark 3 (Integer > 0; **Default = 20**).

Remarks:

1. Grid responses associated with one particular load case are grouped by the specification of DRESP1 entries. From each group, a maximum of NSTR constraints are retained per load case.
2. Element responses are grouped by the property: i.e., all element responses for one particular load case belonging to the set of PIDs specified under ATTi on a DRESPi entry are regarded as belonging to the same region. In superelement sensitivity analysis, if the property (PID) is defined in more than one superelement, then separate regions are defined. A particular stress constraint specification may be applied to many elements in a region generating many stress constraints, but only up to NSTR constraints per load case will be retained.
3. For aeroelastic responses, that is RTYPE = “TRIM, “STABDER,” and “FLUTTER,” the NSTR limit is applied to all DRESP1 IDs that are the same RTYPE and have the same REGION specified.
4. For responses that are not related to grids or elements, that is RTYPE = “WEIGHT,” “VOLUME,” “EIGN,” “FREQ,” “LAMA,” CEIG,” “FRMASS,” “COMP,” and TOTSE,” NSTR is not used. TRS is still applicable.
5. The RTYPE field is set to EQUA if constraints that are associated with DRESP2 entries are to be screened. The RTYPE field is set to DRESP3 if constraints that are associated with DRESP3 entries are to be screened. If the REGION field on the DRESP2 or DRESP3 is blank, one region is established for each DRESP2/DRESP3 entry.
6. If a certain type of constraint exists but no corresponding DSCREEN entry is specified, all the screening criteria used for this type of constraint will be furnished by the default values.
7. Constraints can be retained only if they are greater than TRS. See the footnote 1 under the DCONSTR, 1637 entry for a definition of constraint value.
8. Constraint screening is applied to each superelement.

DCONSTR: Design Constraints

Defines design constraints.

Format:

1	2	3	4	5	6	7	8	9	
DCONSTR	DCID	RID	LALLOW/LID	UALLOW/UID	LOWFQ	HIGHFQ			

Example:

DCONSTR	101	211	0.0	0.0					

Describer	Meaning
DCID	Design constraint set identification number (Integer > 0).
RID	DRESPi entry identification number (Integer > 0).
LALLOW/LID	Lower bound on the response quantity, or the set identification ID of a number of a TABLEDi entry that supplies the lower bound as a function of frequency (Real; Default = -1.0E20).
UALLOW/UID	Upper bound on the response quantity, or the set identification ID of a number of a TABLEDi entry that supplies the upper bound as a function of frequency (Real; Default = 1.0E20).
LOWFQ	Low end of frequency range in Hertz (Real > 0.0; Default = 0.0). See Remark 8.
HIGHFQ	High end of frequency range in Hertz (Real > LOWFQ; Default = 1.0E+20). See Remark 8.

Remarks: Refer to the MSC NASTRAN manual[1]

1. LOWFQ and HIGHFQ fields are functional only for RTYPE with a “FR” or a “PSD” prefix; e.g., FRDISP, or on DRESP2 or DRESP3 entries that inherit the frequency value from these RTYPES. The bounds provided in LALLOW and UALLOW are applicable to a response only when the value of forcing frequency of the response falls between the LOWFQ and HIGHFQ. If the ATTB field of the DRESP1 entry is not blank and these responses are subsequently referenced on a DRESP2 or DRESP3, the LOWFQ and HIGHFQ are ignored when the DCONSTR refers to these DRESP2/DRESP3 responses. LOWFQ/HIGHFQ are not ignored when the DCONSTR refers to a DRESP1 that has a real number in the ATTB field.

DCONADD: Design Constraint Set Combination

Defines the design constraints for a subcase as a union of DCONSTR entries.

Format:

1	2	3	4	5	6	7	8	9	
DCONADD	DCID	DC1	DC2	DC3	DC4	DC5	DC6	DC7	
	DC8	Etc.							

Example:

DCONADD	2000	101	102	103	104	105	106	107	+
+	108	109	110	111	112	113	114	115	

Describer	Meaning
DCID	Design constraint set identification number (Integer > 0).
DCi	DCONSTR entry identification number (Integer > 0).

Remarks: Refer MSC NASTRAN manual[1]

1. The DCONADD entry is selected by a DESSUB or DESGLB Case Control command.
2. All DCi must be unique from other DCi.
3. For PART SE, DCi from different PART SEs can be referenced on a single DCONADD, and only DCONADD in the main Bulk Data section starts with “BEGIN BULK” or “‘BEGIN SUPER=0” and will be considered as part of design constraints. Note that DCONADD entries in “BEGIN SUPER=seid” where seid>0 will be ignored.

PARAM, XYUNIT, #

Unit number for assigning ASCII file defined in ASSIGN statement.

Appendix D: Sample MSC NASTRAN Input Deck

The MSC NASTRAN input deck for the computation of the sensitivity values is prepared in this appendix using a simple cantilevered beam model shown in fig. D1.

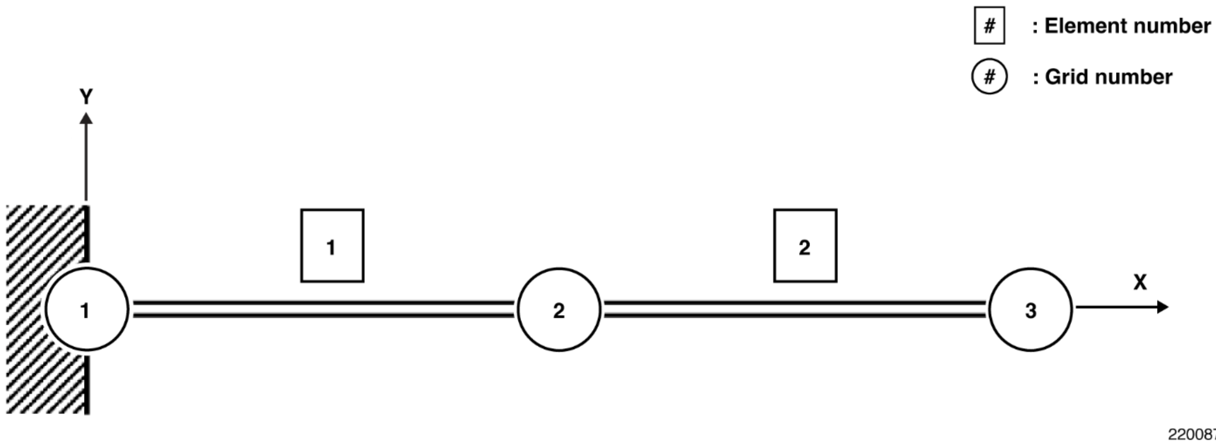

Figure D1. a simple cantilevered beam

The MSC NASTRAN bulk cards for the cantilevered beam model are as follows:

GRID	1		0.	0.	0.				
GRID	2		5.	0.	0.				
GRID	3		10.	0.	0.				
CBAR	1	1	1	2	0.	1.	0.		
CBAR	2	1	2	3	0.	1.	0.		
PBAR	1	1	2.4	10.	200.	5.			
MAT1	1	1.0+7		0.3					
CONM2	41	3		90.	1.0	2.0	3.0		+
+	100.		300.			600.			
SPC1	1	123456	1						
ASET1	123456	2	3						

In this sample model, all the response function and corresponding sensitivity values are saved in an ASCII file, "result.csv" with the following executive and case control commands, as well as a bulk data card.

<u>Executive control command</u>
ASSIGN userfile='results.csv', unit=52, status=unknown, form=formatted

<u>Case control commands</u>
Set 503= 3, 4, 29, 57
DESVAR=503
DSAPRT(FORMATTED, END=SENS)=ALL

<u>Bulk data card</u>
PARAM, XYUNIT, 52

A total of 11 variables have been selected for the design variables in this sample problem. These variables are defined using DESVAR, DVPREL1, and DVCREL1 bulk data cards as follows:

PBAR related design variables:

DESVAR	1	DV001	2.4	0.01	500.				
DESVAR	2	DV002	10.	0.01	500.				
DESVAR	3	DV003	200.	0.01	500.				
DESVAR	4	DV004	5.	0.01	500.				

DVPREL1	1	PBAR	1	4					+
+	1	1.0							
DVPREL1	2	PBAR	1	5					+
+	2	1.0							
DVPREL1	3	PBAR	1	6					+
+	3	1.0							
DVPREL1	4	PBAR	1	7					+
+	4	1.0							

CONM2 related design variables:

DESVAR	29	DV029	90.	0.0001	356.				
DESVAR	43	DV043	1.0	-2.0	5.0				
DESVAR	47	DV047	2.0	-2.0	5.0				
DESVAR	57	DV057	3.0	-2.0	5.0				
DESVAR	5	DV005	100.	0.	1000.				
DESVAR	6	DV006	300.	0.	1000.				
DESVAR	7	DV007	600.	0.	1000.				

DVCREL1	5	CONM2	41	M					+
+	29	1.0							
DVCREL1	6	CONM2	41	X1					+
+	43	1.0							
DVCREL1	7	CONM2	41	X2					+
+	47	1.0							
DVCREL1	8	CONM2	41	X3					+
+	57	1.0							
DVCREL1	9	CONM2	41	I11					+
+	5	1.0							
DVCREL1	11	CONM2	41	I22					+
+	6	1.0							
DVCREL1	10	CONM2	41	I33					+
+	7	1.0							

Response function values in eq. (3) can be obtained using the following bulk data cards:

DRESP1	200	W	Weight						
DRESP1	201	W26	Weight			2	6		
DRESP1	202	W34	Weight			3	4		
DRESP1	203	W15	Weight			1	5		
DRESP1	204	W44	Weight			4	4		
DRESP1	205	W45	Weight			4	5		

DRESP1	206	W55	Weight			5	5		
DRESP1	207	W46	Weight			4	6		
DRESP1	208	W56	Weight			5	6		
DRESP1	209	W66	Weight			6	6		

The following definition of an equation,

DEQATN	901	F(R1,R2) = R1/R2

is needed for the computations of CG locations in eq. (4).

DRESP2	211	Xcg	901						+
+	DRESP1	201	200						
DRESP2	212	Ycg	901						+
+	DRESP1	202	200						
DRESP2	213	Zcg	901						+
+	DRESP1	203	200						

The diagonal terms of the mass moment of the inertia matrix in eqs (5)-(7) are computed using the following commands:

DEQATN	902	F(R1,R2,R3,R4) = R1-R2*(R3**2+R4**2)							
DRESP2	214	Ixx	902						+
+	DRESP1	204	200						+
+	DRESP2	212	213						
DRESP2	216	Iyy	902						+
+	DRESP1	206	200						+
+	DRESP2	213	211						
DRESP2	219	Izz	902						+
+	DRESP1	209	200						+
+	DRESP2	211	212						

Similarly, off-diagonal terms of the inertia matrix are obtained from eqs. (8)-(10) as follows:

DEQATN	903	F(R1,R2,R3,R4) = -R1-R2*R3*R4							
DRESP2	215	Iyx	903						+
+	DRESP1	205	200						+
+	DRESP2	212	211						
DRESP2	217	Izx	903						+
+	DRESP1	207	200						+
+	DRESP2	213	211						
DRESP2	218	Izy	903						+
+	DRESP1	208	200						+
+	DRESP2	213	212						

In this sample case, three natural frequencies and their corresponding mode shapes are computed; therefore, response function values related to natural frequencies and mode shapes are computed using the following bulk data cards:

DRESP1	301	FREQ1	FREQ			1			
DRESP1	302	FREQ2	FREQ			2			

DRESP1	303	FREQ3	FREQ			3			
DRESP1	401	SHAPE1	DISP			123456	**1**	2	+
+	3								
DRESP1	402	SHAPE2	DISP			123456	**2**	2	+
+	3								
DRESP1	403	SHAPE3	DISP			123456	**3**	2	+
+	3								

The response function values should be part of the constraint functions or the objective function to be computed during the MSC NASTRAN run. The following constraint functions are used in this sample model:

DCONSTR	101	211	0.0	0.0					
DCONSTR	102	212	0.0	0.0					
DCONSTR	103	213	0.0	0.0					
DCONSTR	104	214	0.0	0.0					
DCONSTR	105	215	0.0	0.0					
DCONSTR	106	216	0.0	0.0					
DCONSTR	107	217	0.0	0.0					
DCONSTR	108	218	0.0	0.0					
DCONSTR	109	219	0.0	0.0					
DCONSTR	110	301	0.0	0.0					
DCONSTR	111	302	0.0	0.0					
DCONSTR	112	303	0.0	0.0					
DCONSTR	113	401	0.0	0.0					
DCONSTR	114	402	0.0	0.0					
DCONSTR	115	403	0.0	0.0					
DCONADD	2000	101	102	103	104	105	106	107	+
+	108	109	110	111	112	113	114	115	

The following case control commands will select constraint and objective functions:

Case control commands
DESOBJ(MIN) = 200
DESSUB = 2000

References

1. Baruch, M., and Itzhack Y. Bar Itzhack, "Optimal Weighted Orthogonalization of Measured Modes," *AIAA Journal*, Vol. 16, No. 4, 1978, pp. 346–351.

2. Minas, C., and D. J. Inman, "Matching Finite Element Models to Modal Data," *ASME Journal of Vibration and Acoustics*, Vol 112, Issue 1, 1990, pp. 84–92.

3. Berman, A., and E. J. Nagy, "Improvement of a Large Analytical Model Using Test Data," *AIAA Journal*, Vol, 21, No. 8, 1983, pp. 1168–1170.

4. Schwarz, Brian., Mark Richardson, and David L. Formenti, "FEA Model Updating Using SDM," *Journal of Sound and Vibration*, Vol., 41, Issue 10, 2007, pp. 18–23.

5. Heylen, W., and P. Vanhonacker, "An Automated Technique for Improving Model Matrices by Means of Experimentally Obtained Dynamic Data," AIAA Paper 83-0881, 1983.

6. Pak, Chan-gi, “Finite Element Model Tuning Using Measured Mass Properties and Ground Vibration Test Data,” *ASME Journal of Vibration and Acoustics*, Vol. 131, No. 1, Feb. 2009.

7. Pak, Chan-gi, and Shun-fat Lung, “Flutter Analysis of Aerostructures Test Wing with Test Validated Structural Dynamic Model,” *Journal of Aircraft*, Vol. 48, No. 4, 2011, pp. 1263–1272.

8. Pak, Chan-gi, and Samson Truong, “Creating a Test-Validated Finite-Element Model of the X-56A Aircraft Structure,” *Journal of Aircraft*, Vol. 52, No. 5, 2015, pp. 1644–1667.

9. Juneja, V., Raphael Haftka, and Harley Cudney, "Location of Damage in a Space Structure by Contrast Maximization," AIAA Paper 94-1711-CP, 1994.

10. Kim, H., and Theodore Bartkowicz, "Damage Detection and Health Monitoring of Large Space Structures," AIAA Paper 93-1705-CP, 1993.

11. Zimmerman, D. C., and T. Simmermacher, "Model Refinement and System Health Monitoring Using Data from Multiple Static Loads and Vibration Tests," AIAA Paper 94-1714-CP, 1994.

12. Jaishi, B., and Wei-Xin Ren, "Damage Detection by Finite Element Model Updating Using Modal Flexibility Residual," *Journal of Sound and Vibration*, Vol. 290, Issues 1-2, 2006, pp. 369-387.

13. Avitabile, Peter, "Twenty Years of Structural Dynamic Modification - A Review, "*Journal of Sound and Vibration*, Vol. 37, Issue 1, 2003, pp. 14-257.

14. Chen, Gan., "FE Model Validation for Structural Dynamics," Ph.D. thesis, Mechanical Engineering Department, Imperial College London (University of London), London, 2001.

15. Friswell, Michael. L., and J. E. Mottershead, *Finite Element Model Updating in Structural Dynamics*, Kluwer Academic Publishers, Dordrecht, 1996.

16. *MSC NASTRAN: 2018 Quick Reference Guide*, MSC Software Corporation, Newport Beach, California, 2017.

17. O’Callahan, J., P. Avitabile, and R. Riemer, “System Equivalent Reduction Expansion Process (SEREP),” Proceedings of the 7th International Modal Analysis Conference, Las Vegas, Nevada, June 1989, pp. 29–37.

18. Doyle, S., Joe Robinson, Vananh Ho, Grant Ogawa, and Myles Baker, “Aeroelastic Optimization of Wing Structure Using Curvilinear Spars and Ribs (SpaRibs) and SpaRibMorph,” 58th AIAA/ASCE/AHS/ASC Structures, Structural Dynamics, and Materials Conference, Grapevine, Texas, AIAA 2017-1303, January 2017.

19. *ZAERO User’s Manual: Version 9.2*, ZONA Technology, Inc., Scottsdale, AZ, 2016.

20. Haftka, Raphael T., and Manohar. P Kamat, *Elements of Structural Optimization*, Martinus Nijhoff Publishers, Dordrecht, 1985.